JOURNAL OF PETROLOGY | VOLUME 47 | NUMBER 12 | PAGES 2433–2462 | 2006 | doi:10.1093/petrology/egl050

Coexisting High- and Low-Calcium Melts Identified by Mineral and Melt Inclusion Studies of a Subduction-Influenced Syn-collisional Magma from South Sulawesi, Indonesia

MARLINA ELBURG[1,2,3]*, VADIM S. KAMENETSKY[1,4], IGOR NIKOGOSIAN[2,5], JOHN FODEN[6] AND ALEXANDER V. SOBOLEV[1]

[1]MAX PLANCK INSTITUTE FOR CHEMISTRY, GEOCHEMISTRY DIVISION, MAINZ, 55020, GERMANY

[2]FACULTY OF EARTH AND LIFE SCIENCES, DEPARTMENT OF ISOTOPE GEOCHEMISTRY, FREE UNIVERSITY, AMSTERDAM, 1081 HV, THE NETHERLANDS

[3]DEPARTMENT OF GEOLOGY AND SOIL SCIENCE, GHENT UNIVERSITY, KRIJGSLAAN 281 S8, 9000 GHENT, BELGIUM

[4]SCHOOL OF EARTH SCIENCES AND CODES SRC, UNIVERSITY OF TASMANIA, HOBART, TAS 7001, AUSTRALIA

[5]FACULTY OF GEOSCIENCES, UTRECHT UNIVERSITY, UTRECHT, 3508 TA, THE NETHERLANDS

[6]DEPARTMENT OF GEOLOGY AND GEOPHYSICS, UNIVERSITY OF ADELAIDE, ADELAIDE, SA 5005, AUSTRALIA

RECEIVED NOVEMBER 28, 2005; ACCEPTED AUGUST 22, 2006; ADVANCE ACCESS PUBLICATION SEPTEMBER 20, 2006

Mineral and melt inclusions in olivines from the most Mg-rich magma from the southern West Sulawesi Volcanic Province indicate that two distinct melts contributed to its petrogenesis. The contribution that dominates the whole-rock composition comes from a liquid with high CaO (up to 16 wt %) and low Al_2O_3 contents (CaO/Al_2O_3 up to 1), in equilibrium with spinel, olivine ($Fo_{85–91}$; CaO 0·35–0·5 wt %; NiO 0·2–0·30 wt %) and clinopyroxene. The other component is richer in SiO_2 (>50 wt %) and Al_2O_3 (19–21 wt %), but contains significantly less CaO (<4 wt %); it is in equilibrium with Cr-rich spinel with a low TiO_2 content, olivine with low CaO and high NiO content ($Fo_{90–94}$; CaO 0·05–0·20 wt %; NiO 0·35–0·5 wt %), and orthopyroxene. Both the high- and low-CaO melts are potassium-rich (>3 wt % K_2O). The high-CaO melt has a normalized trace element pattern that is typical for subduction-related volcanic rocks, with negative Ta–Nb and Ti anomalies, positive K, Pb and Sr anomalies, and a relatively flat heavy rare earth element (HREE) pattern. The low-CaO melt shows Y and HREE depletion ($Gd_n/Yb_n \leq 41$), but its trace element pattern resembles that of the whole-rock and high-CaO melt in other respects, suggesting only small distinctions in source areas between the two components. We propose that the depth of melting and the dominance of H_2O- or CO_2-bearing fluids were the main controls on generating these contrasting magmas in a syn-collisional environment. The composition of the low-CaO magma does not have any obvious rock equivalent, and it is possible that this type of magma does not easily reach the Earth's surface without the assistance of a water-poor carrier magma.

KEY WORDS: *melt inclusions; mineral chemistry; olivine; syn-collisional magmatism; ankaramites; low-Ca magma*

INTRODUCTION

Arc magmas are mixtures of silicate liquid and crystals that are often assumed to be phenocrysts that crystallized from the enclosing melt. There is, however, increasing evidence that these crystals belong to more than one

*Corresponding author. Present address: Department of Geology and Soil Science, Ghent University, Krijgslaan 281 S8, 9000 Ghent, Belgium. Telephone: +32-9-2644566. Fax: +32-9-2644984. E-mail: Marlina.Elburg@Ugent.be

© The Author 2006. Published by Oxford University Press. All rights reserved. For Permissions, please e-mail: journals.permissions@oxfordjournals.org

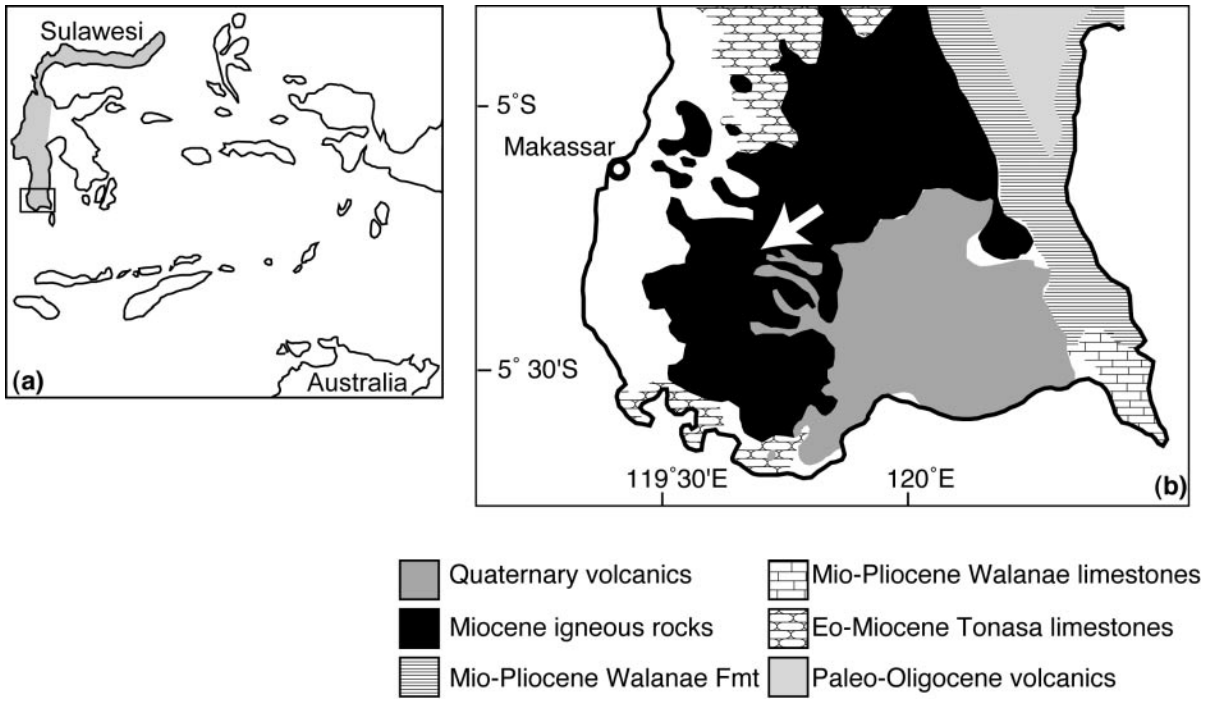

Fig. 1. (a) Sketch map of part of the Indonesian archipelago, including the island of Sulawesi, indicating the location of (b). Grey area indicates the Western Sulawesi Volcanic Province. (b) More detailed map of South Sulawesi, after Elburg & Foden (1999). White arrow indicates sample location (5·251°S, 119·711°E).

population (Tepley *et al.*, 2000; Turner *et al.*, 2003). They may be phenocrysts in equilibrium with melts that are more or less evolved than, but related to, the host liquid; phenocrysts from melts that are genetically unrelated to the host melt; or they may be xenocrysts from the mantle or crust through which the magma ascended. Even if crystals are indeed phenocrysts of the melt in which they occur, it is questionable whether whole-rock analyses represent liquid compositions, as accumulative processes may also have played a role. Whole-rock analyses cannot, therefore, be relied on to obtain information about the composition of mantle-derived melts without careful study of their 'crystal cargo'. For arc-related studies this problem is compounded by the fact that most lavas are too evolved to be in equilibrium with a peridotitic mantle assemblage (Davidson, 1996), and must have been affected by processes such as crystal fractionation, magma mixing, crustal contamination and/or degassing.

Early crystallizing minerals such as forsteritic olivine, magnesium-rich clinopyroxene or spinel are more likely to retain information about the primitive magma from which they crystallized (Clynne & Borg, 1997) than whole-rock compositions do. Better still, these mineral phases sometimes contain melt inclusions, which represent small pockets of (primitive) melt, and these can, when erupted and quenched soon enough after entrapment, be used to study these liquids directly (Kamenetsky & Clocchiatti, 1996; Schiano *et al.*, 2000; Sobolev *et al.*, 2000; Frezzotti, 2001; Kent & Elliott, 2002). We combined the study of mineral compositions and melt inclusions in a collision-related high-Mg arc magma from southern Sulawesi (Indonesia). Both the minerals and their melt inclusions preserve evidence of the existence of distinct primitive melts in the system, which mixed to form the magma we find at the Earth's surface. Importantly, and a major focus of this study, is the identification of a melt component for which no equivalent whole-rock compositions have been reported previously. We argue that this might represent small-degree melts that do not reach the surface without the assistance of a 'carrier magma'.

GEOLOGICAL BACKGROUND

The general tectonic history of the Western Sulawesi Volcanic Province (Fig. 1), from which the studied sample originates, has been described at length by Elburg & Foden (1999) and Elburg *et al.* (2002*b*, 2003). It belongs to the now extinct part of the Indonesian arc, which was active from the Paleocene to the Miocene. The sample, Tnv96-1, belongs to a 6–9 Ma silica-undersaturated suite of ultrapotassic volcanic rocks with pronounced 'continental' isotopic characteristics ($^{87}Sr/^{86}Sr = 0{\cdot}7045–0{\cdot}7061$), indicative of the involvement of subducted continental material in magma genesis. It is a duplicate sample from the same dyke as

sample Tnv11 of Elburg & Foden (1999), which cross-cuts slightly deformed lahar-like deposits of unknown age. This dyke looks homogeneous in the field, and petrographic analysis shows that the mineralogy and texture of the two samples is the same. The chemical composition of Tnv96-1 can therefore be assumed to be the same (within error) as that of Tnv11, which is among the three most mafic samples of the suite (20 wt % MgO; Table 1). It can be classified as being both shoshonitic (1·7 wt % K_2O at 46·7 wt % SiO_2, $K_2O/Na_2O = 1·1$) and ankaramitic (phenocrysts of clinopyroxene and olivine only; $CaO/Al_2O_3 > 1$). Its composition is nepheline-normative (0·6 wt %), with 28 wt % of normative diopside and 36 wt % olivine; normative plagioclase (An_{73}) and orthoclase constitute 22 and 10 wt %, respectively. Its high MgO content, high mg-number [$100 \times Mg/(Mg + Fe_{tot})$] and a mineralogy that is dominated by high mg-number olivine and clinopyroxene crystals (see below) indicate that this sample has undergone little fractionation and is therefore the most likely candidate to give us information about the magma parental to the syn-collisional suite of rocks.

All samples from this suite show typical subduction-related trace element characteristics, with negative anomalies for Nb, Zr and Ti and positive anomalies for Rb, Sr, Pb and the light rare earth elements (LREE) in normalized trace element diagrams. This potassic magmatism took place shortly after collision of the Sula platform with the Western Sulawesi volcanic arc, which brought west-dipping subduction to a halt (Elburg & Foden, 1999). The continental crust underlying Western Sulawesi belongs to Sundaland, and was probably cratonized in the Mesozoic. The area from which the sample originates does not show evidence for underthrusting of allochthonous continental fragments, in contrast to Central Sulawesi (Elburg *et al.*, 2003).

ANALYTICAL TECHNIQUES

Major element mineral and glass analyses were performed on a JEOL 8200 electron microprobe at the Max Planck Institute for Chemistry, using natural mineral standards for calibration. Olivine and spinel were analysed with an accelerating voltage of 20 kV and a current of 20 nA. All other phases were analysed with 15 kV and 12 nA. The beam diameter was 2 μm. To obtain paired analyses of olivines and melt inclusions, olivine analyses were performed at distances of ~30 μm from the melt inclusion to avoid NiO depletion and CaO enrichment of the olivine by diffusional exchange between the two phases (see discussion on LC olivines below).

Trace elements in the melt inclusions were analysed by laser ablation–inductively coupled plasma–mass spectrometry (LA–ICP–MS), using a Finnigan Element 2 with a Merchantek 213 nm laser, and a Cameca 3f ion microprobe, both at the Max Planck Institute for Chemistry. LA–ICP–MS analyses were performed with He as carrier gas. The instrument was tuned to minimize oxide production, which was always less than 1 rel. % of the signal of its element. Raw Th/U ratios of the NIST 612 glass were ~0·91. The laser was operated with a spot size of 60 μm at 6 J/cm^2 and resulted in pits with height:width ratios of one. One run consisted of 60 scans of 1·5 s each, of which the first 17 scans were taken with the laser shutter closed, to determine the blank, which was subtracted from the analysis. The analyses were normalized to the Ca content of the inclusion, which had been determined prior to laser ablation by electron microprobe. Melt inclusions with dimensions smaller than 60 μm were also analysed, in which case part of the enclosing olivine was ablated. This is unlikely to have affected either the relative or absolute trace element abundances measured for the melt inclusion significantly, as olivine has extremely low levels of all trace elements analysed, and very minor contents of the normalizing element Ca. Not all scans were used for all inclusions, as the inclusion was sometimes thinner than 60 μm. In that case, only those scans were used where all elements were above the detection limit. NIST SRM612 glass was used for calibration, but was always analysed at the end of the complete set of analyses, to avoid memory effects for elements that are far lower in the glasses analysed than in the calibration standard (e.g. Ta, Nb, Hf). Secondary standards (Kl2-G and StHs6/80-G; Jochum *et al.*, 2000) were used to check the accuracy of the analyses. Ion microprobe measurements of REE were performed following techniques described by Hellebrand *et al.* (2002). A few inclusions were also analysed for H_2O, TiO_2, Li and B contents by ion microprobe, following analytical techniques published by Gurenko *et al.* (2005).

MINERAL CHEMISTRY

Olivine and clinopyroxene are the most important mineral phases in this sample, and form euhedral crystals. Deformation textures, such as kink bands or undulose extinction, have not been observed in any of the crystals. Chromium-rich spinel occurs as inclusions in olivine and clinopyroxene. Plagioclase, Fe-rich spinel and biotite (rare) occur as microphenocrysts. The groundmass of the sample is largely crystalline, reflecting relatively slow cooling within a dyke. The sample is fairly crystal rich, with large clinopyroxene and olivine crystals constituting 23 and 28 vol. % of the sample, respectively.

Olivine crystals have forsterite (Fo) contents varying between 81 and 94 mol %, although rim compositions can occasionally be as low as 65 mol %. Most compositions, however, lie between 85 and 94 mol % Fo. The olivine analyses scatter widely in diagrams of

Table 1: *Whole-rock, melt and orthopyroxene inclusions and enclosing olivine analyses*

Sample:	Tnv11	ol2000 incl1	ol2009 incl1	ol2076 incl1	ol99 incl2	ol13 incl8
Type:	WR	LC Hy	LC Hy	LC Ne	LC-HC	HC
SiO_2	46·70	52·75	58·10	44·42	58·46	48·23
TiO_2	0·53	0·88	0·87	1·32	0·21	1·05
Al_2O_3	9·12	20·64	19·61	19·28	17·87	14·93
FeO*	9·03	3·82	2·28	3·56	3·33	5·49
MnO	0·16	0·06	0·04	0·02	0·07	0·10
MgO	20·23	5·40	4·15	6·64	3·85	7·86
CaO	10·64	3·37	2·17	12·16	3·33	13·28
Na_2O	1·47	2·72	3·51	3·44	2·89	2·13
K_2O	1·68	5·42	5·80	6·29	4·61	5·06
P_2O_5	0·29	1·05	0·72	0·86	0·64	0·48
Cl		0·68	0·23	0·43	0·37	0·29
F		0·12	0·13	0·23	0·05	0·12
S		0·11	0·01	0·23	0·02	0·12
Total	100·38	96·84	97·52	98·65	95·56	98·96
mg-no.	80·0	71·6	76·5	76·9	67·4	71·8
CaO/Al_2O_3	1·17	0·16	0·11	0·63	0·19	0·89
Cs		8·91	4·44	9·50		3·38
Rb	55	282	137	203		103
Ba	497	1174	513	1070	1421	542
Th	3·69	14·10	5·23	9·28	14·91	4·85
U	1·39	4·09	2·08	3·33		1·56
Nb	1·90	2·93	2·12	3·63		2·41
Ta		0·19	0·09	0·23		0·16
La	12·6	35·0	15·7	35·1	33·7	15·8
Ce	27·9	71·1	31·6	75·9	68·0	32·7
Pb	14·9	14·7	14·3	38·7		21·7
Pr	4·0	9·5	4·0	10·2	7·9	4·4
Sr	750	1639	698	1455	1796	745
Nd	16·8	45·0	16·8	46·0	28·7	19·4
Sm	4·2	10·2	3·3	11·5	4·3	5·2
Zr	57	140	83	106	97	69
Hf		3·83	2·53	2·68		2·19
Eu	1·23	2·55	1·21	3·16		1·51
Gd	3·93	7·79	2·68	10·21	3·35	4·67
Tb	0·54	0·76	0·24	1·09		0·68
Dy	2·65	3·10	1·13	5·83	1·49	3·50
Y	15·1	8·7	3·8	23·5	6·4	17·9
Ho	0·52	0·37	0·10	0·90		0·67
Er	1·28	0·71	0·24	2·20	0·76	1·82
Tm	0·18	0·05	0·05	0·23		0·25
Yb	1·14	0·26	0·22	1·16	0·39	1·68
Lu	0·18	0·03	0·05	0·16		0·21
Olivine						
SiO_2		41·64	40·68	41·66	40·11	39·67
Al_2O_3		0·05	0·03	0·05	0·04	0·03
FeO		8·21	6·84	5·76	12·06	11·06
MnO		0·14	0·10	0·10	0·23	0·22
MgO		51·70	50·94	52·12	48·00	46·90
CaO		0·19	0·16	0·29	0·33	0·52
Cr_2O_3		0·07	0·05		0·07	0·04
NiO		0·39	0·40	0·40	0·25	0·21
Total		102·39	99·20	100·39	101·09	98·64
Fo (%)		91·8	93·0	94·2	87·6	88·3

Table 1: Continued

Sample:	ol24 incl5	ol31 incl3	ol2031 incl1	ol2037 incl3	ol2019 opx	VG2, SC	StHs6/80-G1
Type:	HC-HF	HC-HF	HC-LF	HC-LF	OPX	STD	STD
SiO_2	47·67	47·41	48·47	48·73	55·94	50·7 (0·27)	
TiO_2	0·88	0·71	0·90	0·80	0·02	1·87 (0·02)	
Al_2O_3	14·81	13·97	17·38	16·27	1·27	14·12 (0·07)	
FeO	4·78	4·62	5·81	6·12	5·12	11·8 (0·16)	
MnO	0·08	0·06	0·12	0·14	0·11	0·21 (0·02)	
MgO	9·66	10·79	7·94	8·45	34·40	6·6 (0·10)	
CaO	14·60	15·06	9·57	10·35	1·37	10·92 (0·07)	
Na_2O	2·22	2·20	2·60	2·68	0·05	2·84 (0·05)	
K_2O	4·17	3·23	5·27	5·15	0·01	0·20 (0·01)	
P_2O_5	0·49	0·41	0·61	0·52		0·22 (0·02)	
Cl	0·17	0·26	0·14	0·13		0·033 (0·002)	
F	0·07	0·08	0·09	0·10		0·14 (0·01)	
S	0·08	0·12	0·02	0·04			
Total	99·55	98·77	98·87	99·40	99·00		
mg-no.	78·3	80·6	70·9	71·1	92·3		
CaO/Al_2O_3	0·99	1·08	0·55	0·64			
Cs	3·69		4·31	3·56			1·43
Rb	113		128	102			26·63
Ba	546	853	743	493	3·4		275
Th	5·62	5·12	6·90	4·76	0·04		2·48
U	1·92		2·03	1·66			0·90
Nb	2·32		2·99	2·11			5·94
Ta	0·15		0·17	0·15			0·42
La	17·8	14·6	23·3	15·9	0·09		12·2
Ce	36·1	32·4	41·9	33·6	0·14		24·0
Pb	19·8		19·9	21·0			10·1
Pr	5·0	4·6	6·0	4·3	0·03		3·08
Sr	785	763	971	662	5·15		463
Nd	23·1	20·3	28·2	20·5	0·06		12·8
Sm	5·8	6·4	6·7	4·7	0·07		2·81
Zr	75	65	87	62	0·65		119
Hf	2·12		2·34	1·73			3·21
Eu	1·60		1·83	1·35			0·92
Gd	5·80	6·26	6·14	4·13	0·07		2·69
Tb	0·75		0·82	0·54			0·37
Dy	4·20	4·18	4·55	3·46	0·05		2·41
Y	20·1	21·0	20·2	15·9	0·33		12·21
Ho	0·76		0·79	0·65			0·46
Er	1·97	2·32	2·08	1·72	0·03		1·25
Tm	0·28		0·27	0·18			0·18
Yb	1·75	1·74	1·83	1·79	0·005		1·29
Lu	0·28		0·25	0·31			0·19
Olivine							
SiO_2	41·26	40·12	40·36	40·11	40·17	40·6 (0·25)	
Al_2O_3	0·04	0·03	0·03	0·04	0·04	0·03 (0·01)	
FeO	8·79	8·36	13·48	13·13	8·28	9·50 (0·06)	
MnO	0·16	0·15	0·26	0·29	0·13	0·14 (0·01)	
MgO	50·11	49·28	46·55	45·55	50·01	49·0 (0·3)	
CaO	0·45	0·50	0·44	0·56	0·11	0·09 (0·01)	
Cr_2O_3	0·04	0·03	0·02		0·10	0·01 (0·01)	
NiO	0·24	0·21	0·21	0·19	0·38	0·37 (0·004)	
Total	101·08	98·67	101·36	99·86	99·22		
Fo (%)	91·0	91·3	86·0	86·1	91·5		

WR, whole-rock, from Elburg & Foden (1999); opx, orthopyroxene. Last two columns are analyses for microprobe standards (STD) glass VG2 and San Carlos (SC) olivine (1 S.D.), and LA–ICP–MS secondary standard StHs6/80-G1.

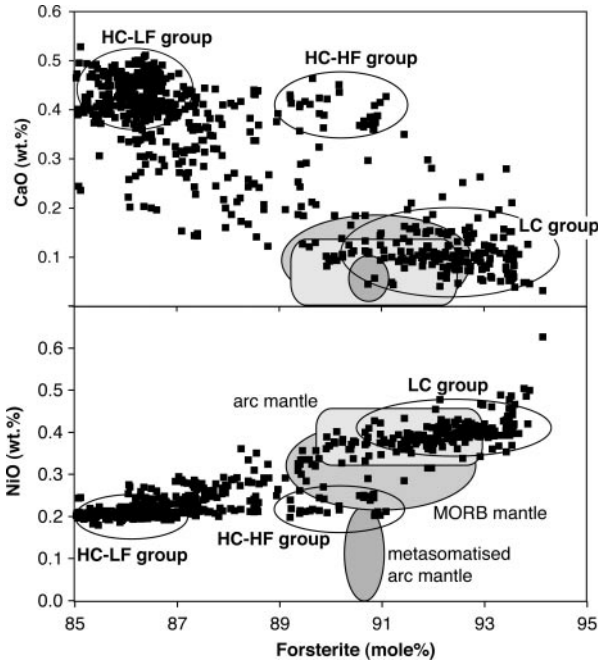

Fig. 2. CaO and NiO content of randomly selected olivines vs their forsterite content (mol %), with fields denoting the different groups of olivines. The one analysis at 0·6 wt % NiO does not represent an analytical outlier. Fields for MORB mantle olivine based on Dick (1989) and unpublished abyssal peridotite database (E. Hellebrand, in preparation); fields for arc mantle and metasomatized arc mantle based on Pearce *et al.* (2000), Griselin (2001) and McInnes *et al.* (2001).

CaO or NiO vs Fo content. This scatter is interpreted to reflect two main groups, with some compositions intermediate between the end-members (Fig. 2). One group has on average higher Fo (92–94), low CaO (0·05–0·2 wt %) and high NiO contents (0·35–0·5 wt %, one crystal with 0·63 wt %; low-calcium group; LC); the second group has lower average Fo, high CaO (0·35–0·5 wt %) and low NiO contents (<0·3 wt %). The latter group can be further subdivided into a small population of olivines with Fo between 90 and 92 (high-calcium, high-forsterite group; HC-HF) and the majority of crystals with Fo 85–87 (high-calcium, low-forsterite group; HC-LF). The intermediate compositions between the HC and LC groups are denoted as LC-HC olivine crystals; those intermediate between HC-HF and HC-LF are referred to as transitional HC olivine crystals. LC olivine crystals are somewhat less common than HC-LF olivines, and HC-HF olivines make up less than 5% of the total population. LC olivine crystals always show a smooth increase in CaO and decrease in NiO contents towards their rims (Fig. 3); a decrease in Fo content is also observed but is not as pronounced, and resembles the zoning seen in the HC olivines. The latter olivine crystals show only a small increase in CaO and decrease in the (already low) NiO contents towards their rims.

Spinel occurs as inclusions in all types of olivine phenocrysts, but is least common in the LC olivines. A good correlation exists between the forsterite content of the olivine and the $Mg/(Mg + Fe^{2+})$ ratio of the enclosed spinel (Fig. 4c). Cr-numbers [$100 \times Cr/(Cr + Al)$] of the spinels in the LC olivine crystals are marginally higher than those in HC-HF olivines (79–82 vs 71–74), whereas those in the HC-LF olivine crystals, which occur most frequently, show a wide variation, with the majority falling between 50 and 60. TiO_2 contents of the latter range up to 1·5 wt %, whereas the spinels in the LC and HC-HF olivine crystals reach only 0·8 wt %. Calculated equilibration temperatures, following Ballhaus *et al.* (1991), between olivine and spinel lie around 1000°C for LC and around 1100°C for HC olivines (Table 2). Oxygen fugacities at these temperatures lie 1–3 log units above the fayalite–magnetite–quartz buffer.

Clinopyroxene phenocrysts show a wide variation in mg-number between 71 and 93. Cr_2O_3 contents vary between 0 and 1 wt %, showing a positive correlation with mg-number, but a wide range of Cr contents is seen at high mg-number (Fig. 5). Negative correlations exist between mg-number on the one hand and Al_2O_3 and TiO_2 on the other, with the most magnesium-rich clinopyroxenes containing as little as 0·05 wt % TiO_2 and 1 wt % Al_2O_3. Clinopyroxene also occurs as inclusions in HC-LF olivines (Table 3); vice versa, HC-LF olivine inclusions are also found within clinopyroxene crystals. The chemical composition of clinopyroxene crystals enclosed within HC-LF olivine is indistinguishable from that of analysed clinopyroxene phenocrysts, except when the inclusions contain spinel in contact with clinopyroxene; in this case subsolidus equilibration appears to have taken place, depleting the clinopyroxene in Ti and Al and causing an enrichment in Cr. Clinopyroxene inclusions were not seen in HC-HF olivine crystals, but this may be a result of the scarcity of these olivines.

Orthopyroxene does not occur as a phenocryst phase, but is found as inclusions in LC olivine crystals. The mg-number of the orthopyroxene is similar to that of the surrounding olivine (Table 3). CaO and Al_2O_3 contents vary up to 1·5 wt % and 2·5 wt %, respectively, and TiO_2 contents are no higher than 0·16 wt %. Cr_2O_3 contents are positively correlated with Al_2O_3 contents and reach 1%.

Biotite microphenocrysts have a variable composition, with mg-number between 35 and 60, and TiO_2 contents between 0·6 and 6·2 wt %. Cl contents are 0·1 wt % or less, and F contents vary between 1 and 1·9 wt %.

Very rare near-spherical Fe–Ni sulphide inclusions were observed in LC olivines.

Plagioclase microphenocrysts have an anorthite content of 48–75 mol %, and the orthoclase component is less than 6 mol %.

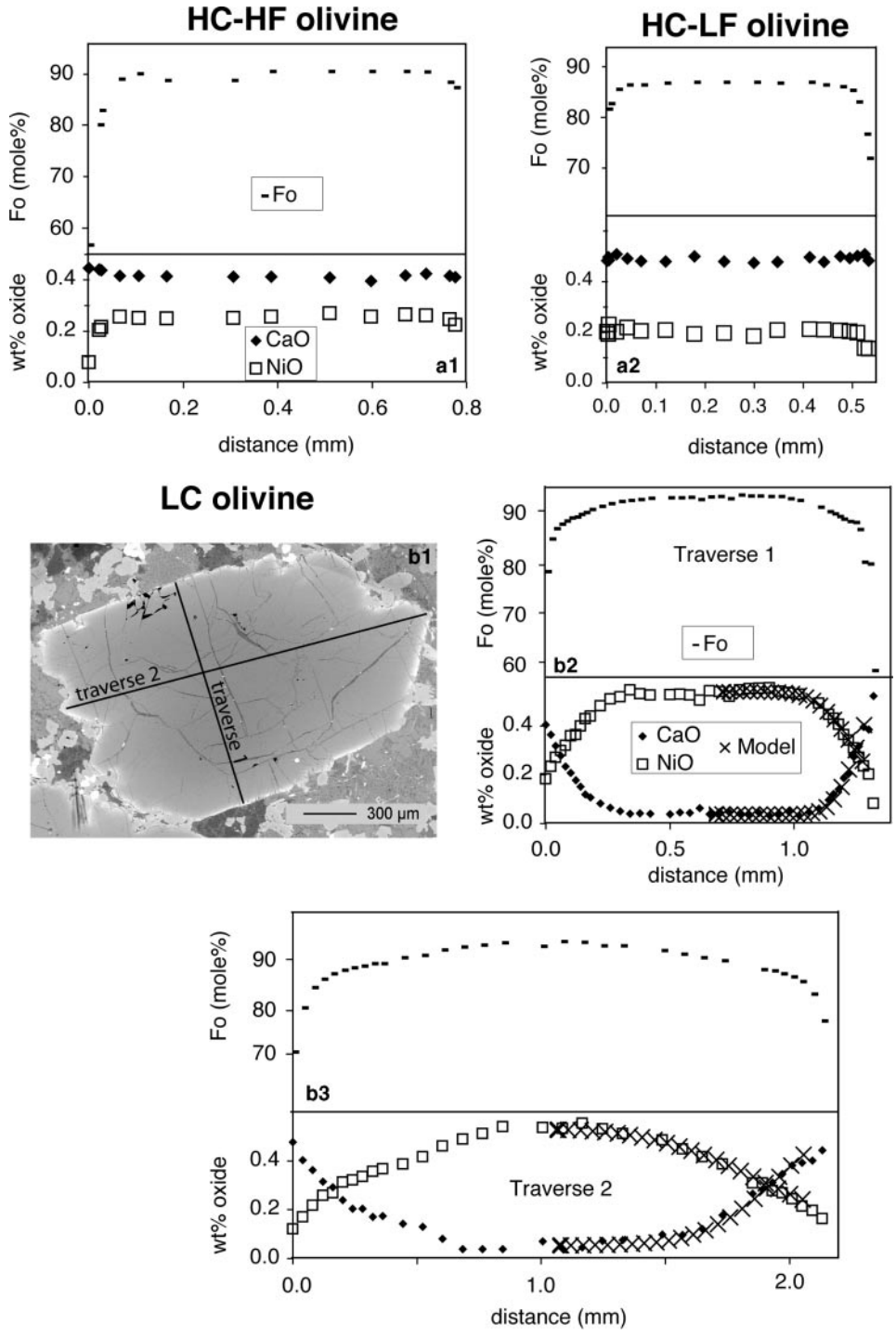

Fig. 3. (a1) NiO, CaO (wt %) and mol % Fo of rim-to-rim traverse of an HC-HF olivine crystal. (a2) Rim-to-rim traverse of an HC-LF olivine crystal. (b1) Backscattered electron image of an LC olivine phenocryst, with location of two electron microprobe traverses. The euhedral shape of the crystal indicates that traverse 2 is close to the crystallographic *c*-axis, along which diffusion is the fastest. (b2) NiO, CaO (wt %) and Fo mol % along traverse 1 in (b1); ×, results of the diffusion profile modelling. (b3) NiO, CaO (wt %) and Fo mol % along traverse 2 in (b1). The NiO and CaO half-profiles have been modelled as diffusion from a sphere into a homogeneous liquid, neglecting simultaneous overgrowth of high-Ca olivine and the ovoid shape of the crystal. Parameters for the modelling are D_{Ni} *c*-axis $= 3 \times 10^{-10}$ mm^2/s; D_{Ca} *c*-axis $= 1{\cdot}5 \times 10^{-10}$ mm^2/s; D_{Ni} other axis $= 4 \times 10^{-11}$ mm^2/s; D_{Ca} other axis $= 1{\cdot}8 \times 10^{-11}$ mm^2/s; C_0 NiO $= 0{\cdot}55\%$; C_s NiO $= 0{\cdot}27\%$; C_0 CaO $= 0{\cdot}04\%$; C_s CaO $= 0{\cdot}39\%$; $t = 5$years.

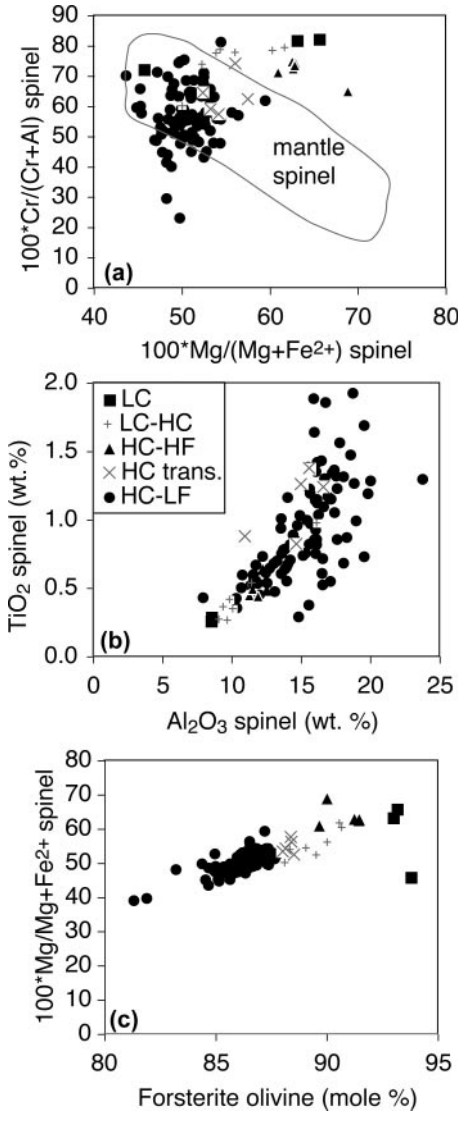

Fig. 4. Electron microprobe analyses of spinel enclosed in olivine. (a) Cr-number vs mg-number, showing that most of the spinels within LC and HC-HF olivine crystals fall outside the field of mantle spinels. (b) TiO_2 vs Al_2O_3 content, showing the low contents of Al_2O_3 and TiO_2 for the spinel crystals enclosed in LC and LC-HC olivine. (c) Mg-number of spinel vs forsterite content of enclosing olivine. It is unclear why the one LC olivine-hosted spinel has lower mg-number.

Diffusion profile modelling of LC olivine

The HC and LC olivine crystals both show decreasing forsterite contents towards the rims of the crystals, but their profiles for NiO and especially CaO are very different (Fig. 3). The HC olivine crystals have high CaO contents in the core of crystals, and show a very moderate increase in CaO content towards the rim of the crystals, which may be followed by a decrease (Fig. 3a2). The LC olivine crystals have very low CaO contents in the core, which show a pronounced increase towards the rim of the crystals. The length scale over which the increase in CaO takes place in LC olivine is larger than in HC olivine. This increase in CaO is matched by a decrease in NiO in the LC olivine. The contrasting length scales of the change in CaO and NiO content between HC and LC olivine suggest that two different mechanisms may be responsible, i.e. quench crystallization for HC olivine crystals and re-equilibration with a contrasting magma for the LC olivine crystals.

To investigate the cause of the strong decrease in NiO and increase in CaO contents towards the rims of the LC olivine crystals, several microprobe traverses were measured over these crystals. The distribution of CaO and NiO along profiles of the LC olivine crystals strongly resemble diffusion profiles (Fig. 3b2 and b3), and could therefore allow us to calculate the time elapsed since these crystals were incorporated in a melt with contrasting composition. We used the Ni and Ca data provided by Petry *et al.* (2004) at 1250°C, and the solution to the diffusion equation for a sphere given by Albarède (1995, p. 449):

$$C(r,t) = C_s + (C_0 - C_s)\left[1 + \frac{2a}{\pi r}\sum_{n=1}^{\infty}\frac{(-1)^n}{n}\sin n\pi\frac{r}{a}\exp\left(-n^2\pi^2\frac{Dt}{a^2}\right)\right].$$

In this formula the parameter a represents the radius of the sphere, r is the distance from the centre of the sphere, C_0 is the original concentration of the element within the sphere (crystal), and C_s is the concentration of the element in the infinite well-stirred medium surrounding the crystal. This solution was expanded from $n = 1$ to $n = 47$, which is well beyond any measurable change in concentration. However, diffusion is unlikely to have been the only process acting upon these olivine crystals, as the high-Ca magma itself was also saturated in olivine, and crystal growth is likely to have been operational at the same time as diffusion. In an attempt to avoid this complication, the diffusional profiles used for modelling were cut off at a certain distance from the rim, where the forsterite contents displayed a sharp drop-off. It is possible that this only accounted for quench crystallization, so the results can only be considered to give us an order of magnitude impression of the time between incorporation of the low-Ca olivine crystals and intrusion of the magma. The original concentration of the crystal was taken to be the same as the concentration in the core of the crystal; the 'infinite reservoir' was given the same concentration as the outermost rim of the modelled crystal. Because the data are only approximate, we did not determine the exact orientations of the olivine crystals, which would be necessary to obtain precise age information (Costa-Rodriguez & Chakraborty, 2004), as

Table 2: *Electron microprobe analyses of spinels and enclosing olivines*

Sample:	151·1	47·1	48·1	92	18	180	104	13·1	70·1	82·1	114·1	134·1	141·1	145·1	84	147	178
Group:	LC	LC-HC	LC-HC	LC-HC	LC-HC	HC-HF	HC	HC-LF	HC-LF	HC-LF	HC-LF	HC-LF	HC-LF	HC-LF	HC-LF	HC-LF	HC-LF
Spinel																	
Al_2O_3	8·55	16·15	11·45	9·10	9·85	12·21	10·98	16·13	23·75	18·27	12·52	17·10	16·68	15·54	17·77	7·90	14·41
TiO_2	0·29	0·98	0·54	0·27	0·42	0·64	0·88	1·12	1·30	0·87	0·54	0·55	1·30	0·38	1·56	0·43	0·89
FeO*	19·60	32·49	26·14	26·67	21·57	26·25	27·85	37·14	45·44	40·72	34·80	34·08	35·87	37·98	32·74	27·96	37·60
MnO	0·28	0·36	0·33	0·34	0·26	0·26	0·29	0·32	0·36	0·33	0·33	0·29	0·32	0·29	0·33	0·29	0·33
MgO	13·07	10·53	10·81	11·06	12·39	13·00	11·80	11·10	10·75	11·71	10·05	12·05	11·72	11·74	11·43	11·13	11·23
Cr_2O_3	56·87	36·21	48·27	50·08	53·05	45·27	46·56	31·30	14·88	25·09	38·90	33·96	31·40	32·07	33·29	51·21	32·93
NiO	0·12	0·17	0·11	0·12	0·14	0·11	0·12	0·20	0·23	0·21	0·13	0·15	0·20	0·18	0·14	0·11	0·17
V_2O_3	0·04	0·09	0·05	0·06	0·03	0·09	0·08	0·11	0·33	0·17	0·08	0·14	0·14	0·12	0·15	0·06	0·12
ZnO	0·13	0·15	0·15	0·09	0·10	0·10	0·08	0·09	0·09	0·07	0·10	0·06	0·09	0·09	0·12	0·11	0·06
Total	99·38	97·54	98·41	98·27	98·12	98·63	99·03	97·88	97·90	97·93	97·78	98·70	98·13	98·71	98·06	99·53	98·13
100Cr/(Cr + Al)	81·7	60·1	73·9	78·7	78·3	71·3	74·0	56·5	29·6	47·9	67·6	57·1	55·8	58·1	55·7	81·3	60·5
Fe^{3+}/Fe^*	0·31	0·42	0·33	0·38	0·33	0·43	0·41	0·51	0·55	0·57	0·47	0·51	0·51	0·56	0·44	0·41	0·53
$Mg/(Mg + Fe^{2+})$	63·1	50·1	52·3	54·4	60·3	60·9	56·1	52·2	48·2	54·3	49·1	56·4	54·4	55·7	52·5	54·4	53·1
Olivine																	
SiO_2	40·68	40·38	40·47	40·42	40·68	40·77	40·64	39·95	39·62	39·86	39·97	40·25	40·29	40·15	40·44	40·06	40·13
Al_2O_3	0·03	0·05	0·04	0·03	0·03	0·03	0·03	0·03	0·03	0·04	0·03	0·04	0·04	0·02	0·01	0·03	0·03
FeO	6·93	11·53	10·20	10·68	9·15	10·08	11·22	12·90	15·96	12·75	14·03	13·01	12·24	12·97	12·61	12·33	13·30
MnO	0·11	0·22	0·18	0·19	0·16	0·20	0·23	0·27	0·33	0·27	0·29	0·26	0·26	0·30	0·24	0·26	0·29
MgO	51·69	47·96	48·93	48·83	49·96	48·98	48·07	46·84	44·33	47·19	45·86	46·80	47·40	46·70	46·84	47·38	46·57
CaO	0·19	0·29	0·32	0·18	0·23	0·43	0·41	0·47	0·35	0·43	0·49	0·40	0·46	0·46	0·42	0·42	0·40
Cr_2O_3	0·15	0·10	0·08	0·07	0·33	0·03	0·07	0·05	0·01	0·16	0·09	0·03	0·07	0·06	0·02	0·17	0·04
NiO	0·39	0·27	0·28	0·31	0·34	0·22	0·22	0·20	0·19	0·22	0·21	0·20	0·22	0·20	0·21	0·24	0·22
Total	100·16	100·80	100·50	100·71	100·89	100·73	100·88	100·72	100·82	100·91	100·97	100·98	100·97	100·86	100·80	100·89	100·99
Fo	93·0	88·1	89·5	89·1	90·7	89·7	88·4	86·6	83·2	86·8	85·4	86·5	87·3	86·5	86·9	87·3	86·2
T (°C)	946	912	919	1014	1022	1088	1076	1047	1012	1069	1055	1104	1054	1133	998	1131	1114
ΔFMQ	1·8	2·5	1·8	1·9	1·5	2·1	2·0	2·8	3·1	3·1	2·3	2·5	2·8	2·8	2·4	1·8	2·7

Analysed spinels were in contact with olivine only, not associated with glass or pyroxene inclusions. Spinel totals not corrected for presence of Fe^{3+}. Equilibration temperatures between olivine and spinel and oxygen fugacities calculated following Ballhaus *et al*. (1991).

diffusion is approximately six times faster along the *c*-axis than along the other two crystallographic axes (Petry *et al.*, 2004). In the case where we measured two diffusional profiles orthogonal to each other, and where the shape of the olivine crystal indicated that one must have been subparallel to the *c*-axis, it is obvious that diffusivity must have been faster along the *c*-axis. The modelling indicates that the crystals must have resided in the high-Ca magma for 5–10 years. In the modelling for the crystal in Fig. 3, the best result was obtained if the diffusion coefficients for Ni and Ca were 7·5 and 8·3 times faster along the traverse subparallel to the *c*-axis than orthogonal to this direction; this is a somewhat higher ratio than the six-fold value reported in the literature (Petry *et al.*, 2004). Moreover, the diffusion coefficients for Ni were only twice that of Ca, whereas they are supposed to be close to an order of magnitude different. Although this may reflect the fact that the processes acting on the crystal cannot be approximated by diffusion only, it could also mean that the physical conditions under which diffusion took place were different from those in the experiments from which the diffusion coefficients were determined.

Although this modelling will only be an approximation of the processes that affected the LC olivine crystals, it indicates that the LC olivine crystals may have been incorporated within the HC magma, which constitutes the bulk of the sample and with which the LC olivines were clearly not in equilibrium with respect to CaO and NiO content, several years before the magma intruded to form the dyke that was sampled.

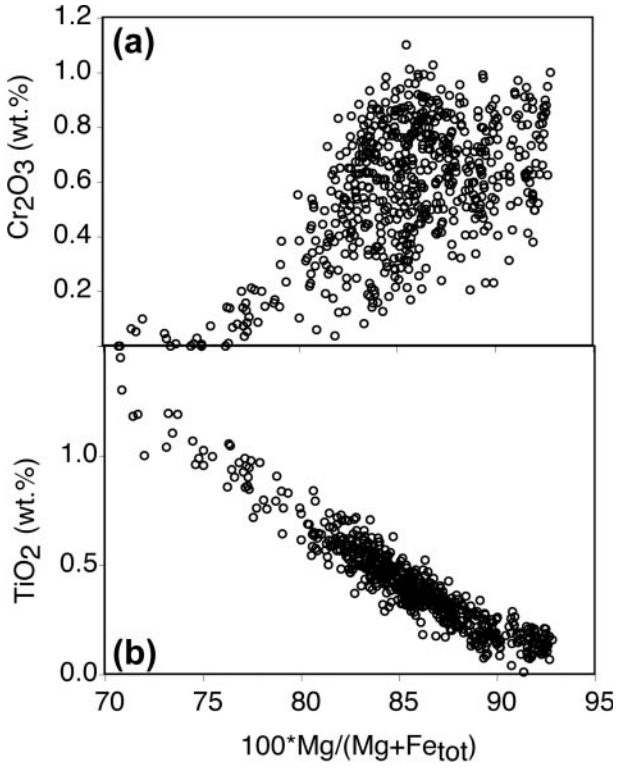

Fig. 5. Electron microprobe analyses of clinopyroxene phenocrysts, with (a) Cr_2O_3 and (b) TiO_2 vs mg-number [$100Mg/(Mg + Fe_{tot})$].

MELT AND FLUID INCLUSION DESCRIPTION

Melt inclusion shape

The three groups of olivine crystals all contain melt inclusions, but those within the HC olivine crystals are significantly larger than those in the cores of the LC olivine crystals, which do not exceed 30 μm diameter. Some LC olivine crystals also contain micro-inclusions of ~0·3 μm, consisting of a tiny spinel, a bubble and some glass. When present, these inclusions are so numerous that they give the crystal a cloudy appearance. Only in one olivine (sample 2009) did several inclusions occur in a single plane, resembling a healed crack through the crystal. All other inclusions analysed occurred as discrete bodies, and were therefore interpreted to be primary inclusions, following the criteria set by Roedder (1984). Their shape was generally spherical or ovoid. Inclusions in LC olivines sometimes have a halo of small inclusions around them, and this arrangement was interpreted as indicating decrepitation of the inclusion during decompression.

Fluid inclusions

A selection of 12 fluid inclusions within the three groups of olivine crystals was studied using a heating–freezing stage, to constrain their freezing and homogenization temperatures, as these can give information on the composition of the volatile phase and the pressure at which they have been trapped (Roedder, 1984). The heating–freezing experiments showed that the ice within the bubble thawed at $-56{\cdot}4 \pm 0{\cdot}9$°C. This melting temperature is indicative of virtually pure CO_2. This result was checked by Raman spectroscopy, which gives information on the molecular bonds present within materials (Burke, 2001). This method yielded peaks of variable intensity at 1288 and 1390 cm^{-1}, which are indicative for CO_2. No evidence was found for the presence of an H_2O-rich fluid, but one inclusion in an LC olivine that had not been reheated yielded a small peak at 2918 cm^{-1}, indicating the presence of minor CH_4.

Homogenization of the volatile phase in the bubbles was hard to observe during heating–freezing experiments, and only one experiment gave an unambiguous result of homogenization into the vapour phase at 27·2°C. This was measured on a fluid inclusion within a rehomogenized melt inclusion within an olivine crystal with characteristics transitional between HC and LC olivine (Fo_{87}, CaO 0·20 wt %). Fluid-only inclusions were measured in two LC olivines which had not been reheated. In these cases, the phase into which homogenization took place was probably vapour (at 10°C) and liquid (at 18°C). Assuming a pure CO_2 fluid and using the program LONER18 (Bakker, 2003), these homogenization conditions indicate pressures at an assumed temperature of 1250°C of 98 MPa, 43 MPa and 508 MPa, respectively. This wide range of pressures is probably a reflection of the fact that the olivines did not behave as perfect containers, which is also indicated by the decrepitation marks described above. However, the one result of ~5 kbar, although hardly statistically relevant, may suggest that crystallization started at significant depth; this is similar to depths obtained by the same method for the Canary Islands (Nikogosian *et al.*, 2002).

Melt inclusion rehomogenization

All melt inclusions were recrystallized and therefore had to be rehomogenized before analysis. One set of olivines was doubly polished and reheated under an optical microscope using a Vernadsky-type heating stage (Sobolev *et al.*, 1980) at the Free University of Amsterdam. Full homogenization was not achieved, as a bubble persisted in all inclusions after disappearance of the last daughter mineral, accounting for up to 36 vol. % of the inclusion. Large bubbles were mostly present in both the hypersthene- and nepheline-normative (see below) inclusions within LC olivines, whereas those in HC olivines were less pronounced. No correlation was noted between the composition of the melt inclusions

Table 3: *Electron microprobe analyses of clino- and orthopyroxenes and enclosing olivine*

Sample:	265	332	344	403	403	641	664	668	932	944	2201-2	88-1
Pyroxene												
SiO_2	52·24	52·72	52·28	52·38	51·34	56·95	57·09	57·85	57·16	57·75	57·87	57·98
TiO_2	0·11	0·11	0·16	0·16	0·22	0·10	0·05	0·08	0·12	0·09	0·03	0·09
Al_2O_3	2·33	1·65	2·02	2·36	2·53	0·64	1·09	0·25	0·98	0·21	0·65	1·46
FeO	4·64	3·84	4·46	4·55	4·53	7·31	5·29	6·81	4·85	4·76	4·46	5·00
MnO	0·09	0·09	0·12	0·12	0·10	0·18	0·12	0·19	0·11	0·09	0·09	0·07
MgO	16·20	16·73	16·41	16·35	16·30	33·10	34·29	33·53	34·79	35·71	35·89	34·18
CaO	23·23	22·98	22·64	22·71	22·86	1·22	1·37	1·36	1·28	0·71	0·58	1·25
Na_2O	0·23	0·24	0·29	0·26	0·28	0·16	0·05	0·08	0·04	0·07	0·01	0·03
K_2O	0·00	0·00	0·00	0·01	0·00	0·01	0·01	0·00	0·01	0·00	0·01	0·00
Cr_2O_3	0·82	0·95	0·99	0·98	1·13	0·16	0·40	0·22	0·25	0·13	0·53	n.a.
NiO	0·01	0·06	0·05	0·01	0·05	0·07	0·12	0·11	0·13	0·11	n.a.	n.a.
Total	99·9	99·4	99·4	99·9	99·3	99·9	99·9	100·5	99·7	99·6	100·1	100·1
100Mg/(Mg + Fe*)	86·2	88·6	86·8	86·5	86·5	89·0	92·0	89·8	92·7	93·0	93·5	92·4
100Cr/Cr + Al)	19·1	27·8	24·8	21·8	23·1	14·2	19·7	36·6	14·6	29·6		
Olivine												
SiO_2	39·64	39·43	39·02	39·40	39·39	39·96	40·32	40·54	40·50	40·16	40·81	40·49
Al_2O_3	0·04	0·02	0·02	0·02	0·03	0·03	0·03	0·02	0·03	0·01	0·05	0·02
FeO	13·25	12·78	13·37	13·44	13·25	11·36	7·83	10·39	8·09	7·12	7·83	7·82
MnO	0·29	0·27	0·25	0·28	0·27	0·21	0·11	0·19	0·14	0·08	0·11	0·11
MgO	46·78	46·54	45·82	46·31	46·03	47·90	50·35	49·38	50·22	50·93	49·86	51·31
CaO	0·44	0·40	0·42	0·42	0·41	0·19	0·13	0·20	0·12	0·07	0·10	0·09
Cr_2O_3	0·04	0·08	0·04	0·06	0·07	0·03	0·06	0·04	0·07	0·04		0·06
NiO	0·21	0·21	0·21	0·21	0·21	0·29	0·40	0·33	0·39	0·43	0·42	0·38
Total	100·7	99·7	99·1	100·1	99·6	100·0	99·2	101·1	99·6	98·8	99·2	100·3
Fo%	86·3	86·6	85·9	86·0	86·1	88·3	92·0	89·4	91·7	92·7	91·9	92·1

All analyes are an average of two or three individual spot analyses. n.a., not analysed.

and its bubble size. The presence of high-pressure CO_2 in some inclusions (see above) indicates that at least some of the bubble volume can be accounted for by the presence of a volatile phase. Most inclusions also contained a spinel crystal, which made up between 2 and 38 vol. % of the total inclusion. The size of this crystal indicates that it cannot be a daughter crystal, crystallized from the trapped melt. It is more likely that the spinel and the melt were trapped at the same time. It is possible that nucleation of a spinel on a growing olivine crystal may have been the cause of melt entrapment in the first place. Partial rehomogenization temperatures ranged from 1100 to 1250°C, with no clear distinction between the different groups of host olivines. This is the best estimate for the temperature at which the melt fraction became trapped in the olivine host. These temperatures are somewhat higher than given by the olivine–spinel geothermometer (Table 2), indicating that the crystals did not erupt immediately after trapping the melt inclusion, but spent a significant amount of time at lower temperatures. This is also suggested by the modelling of Fe-diffusion profiles in olivine around the inclusions (see below).

Two other sets of melt inclusion-bearing olivines were rehomogenized, by heating in a vertical gas-mixing furnace at 1250°C for 3–10 min [University of Heidelberg, Germany (CO/CO_2 = 0·9/0·1) and the University of Tasmania, Australia (Ar atmosphere)]. These inclusions were quenched in water. In some inclusions, homogenization was found to be incomplete, as olivine crystals were present in the inclusion after quenching. After rehomogenization, the olivines were mounted in epoxy and polished to expose the melt inclusions for analysis by electron microprobe, secondary ionization mass spectrometry (SIMS) and LA–ICP–MS.

MELT INCLUSION COMPOSITIONS

Selected melt inclusion compositions are given in Table 1, and the full dataset is available as an Electronic

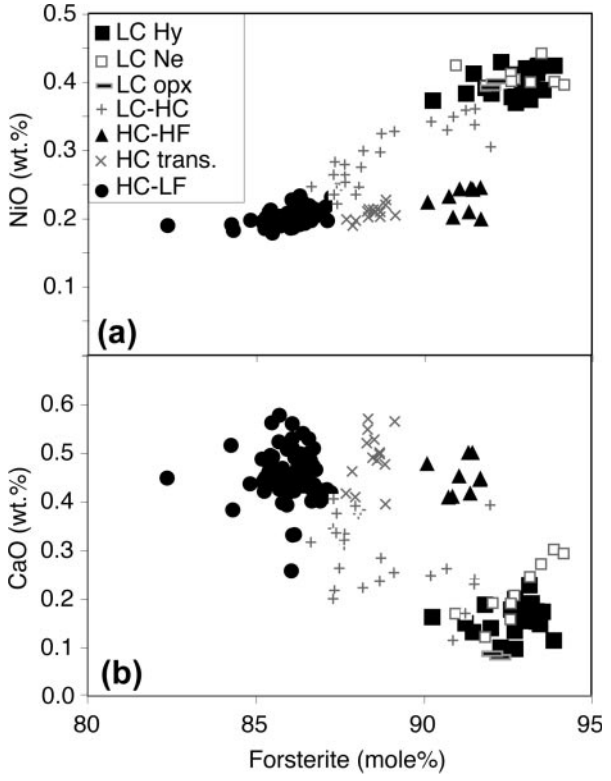

Fig. 6. (a) NiO (wt %) and (b) CaO (wt %) contents against mol % forsterite of the olivines in which melt inclusions have been analysed, showing the compositions of the different groups. Divisions are based on the NiO vs forsterite content of the olivine, apart for the subdivision of the LC-olivine-hosted inclusions, based on their normative mineralogy (hypersthene- or nepheline-normative), and two thin melt rims next to orthopyroxene inclusions within LC olivine (LC opx). These diagrams form the basis for the grouping of the olivine crystals and their melt inclusions: LC, low calcium; HC-HF, high calcium, high forsterite; HC-LF, high calcium, low forsterite; HC trans., high calcium (transitional between HC-HF and HC-LF); LC-HC, transitional between LC and HC.

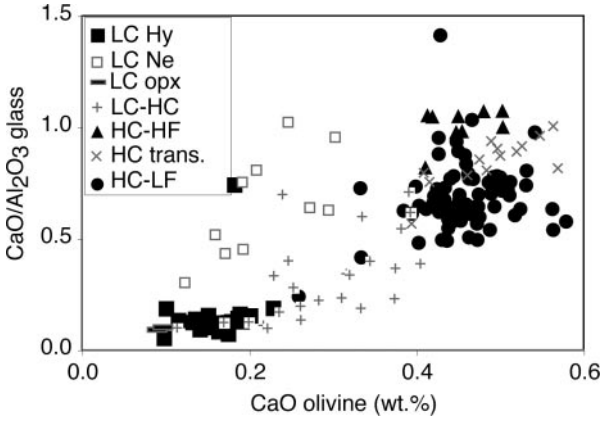

Fig. 7. CaO/Al_2O_3 ratio of the melt inclusions glass vs the CaO content (wt %) of enclosing olivine. Inclusions in HC olivine crystals have significantly higher CaO/Al_2O_3 ratios than the hypersthene-normative inclusions in LC olivine, with intermediate ratios for the inclusions in olivines transitional between the two main groups.

Appendix in MS Excel format (http://www.petrology.oxfordjournals.org). For ease of discussion, the melt inclusions have been divided into several groups, mainly based upon the forsterite and Ni content of the enclosing olivine (Fig. 6a). Most inclusions analysed were found within HC-LF olivine crystals, as this type of olivine is the most abundant and contains large inclusions. Few came from HC-HF olivine crystals, in keeping with the scarcity of these crystals. The inclusions in LC olivine crystals have been subdivided on the basis of their being hypersthene (LC-Hy) or nepheline-normative (LC-Ne) (see below). Not all olivines fall within the three main groups (LC, HC-HF, HC-LF); some are transitional between HC and LC olivine (indicated as LC-HC inclusions), and others fall between the low- and the high-forsterite groups of HC olivine (indicated as transitional HC inclusions in following diagrams and discussions). Had the Fo and calcium content of the olivine crystals been taken as a basis for subdivision, the groups would have remained largely the same (Fig. 6b). Two glasses adjacent to orthopyroxene inclusions within LC olivines are indicated separately in Fig. 6 (denoted as LC-opx). These melt rims are no more than a few microns thick and their volume is only 10% of that of the associated orthopyroxene (in a two-dimensional view), and it is possible that boundary effects during trapping may have influenced their composition.

We will first present the major element composition of the inclusions, uncorrected for any post-entrapment equilibration processes. After this, we will discuss the effects of equilibration with the host olivine.

Major elements

Compositions of melt inclusions are shown in Table 1 and their major element composition has been plotted in Figs 7 and 8. The composition of most melt inclusions is broadly related to that of the enclosing olivine (Fig. 7, Table 1): HC-HF olivine crystals contain melt inclusions with CaO/Al_2O_3 ratios around one, HC-LF inclusions have CaO/Al_2O_3 0·5–1 (apart from one inclusion with an unusually high and as yet unexplained CaO/Al_2O_3 ratio of 1·42), and nearly all hypersthene-normative inclusions in LC and LC-HC olivine crystals fall in the range 0·05–0·4. Ten of the inclusions from the LC-Hy group were analysed in a single crystal, olivine sample 2009, in which the inclusions were located in a plane. These 10 inclusions are very similar, with a standard deviation between 1 and 12 rel. % for all oxides above 0·1%. Considering the correlation between the composition of the melt inclusions and that of the enclosing olivine, it is highly likely that the melt inclusions

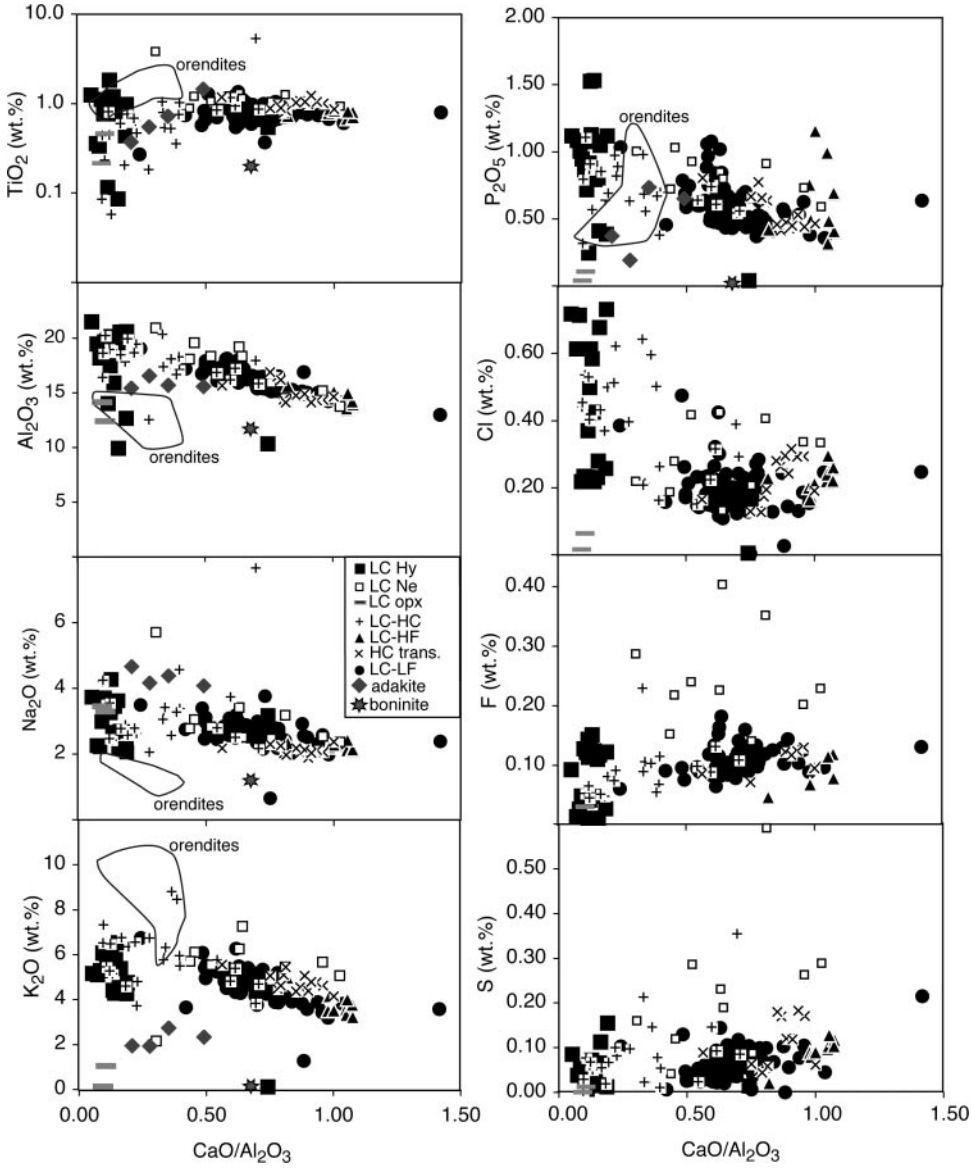

Fig. 8. Variation of major and minor oxides and elements vs the CaO/Al_2O_3 ratio of the glass (uncorrected data). Traditional Harker diagrams cannot be used, because the measured FeO, MgO and SiO_2 contents of the melt inclusions are not representative of the original concentrations of these oxides. (Note log-scale for TiO_2 *y*-axis.) The large scatter seen in a non-volatile element such as P_2O_5 demonstrates that within-group variability is not reflecting simple crystal fractionation processes. Field for Italian orendites from Peccerillo *et al.* (1988). The four 'adakite' analyses are, in order of increasing SiO_2 content: average low-silica adakite, sanukitoid, high-silica adakite and <3 Ga TTG (Martin *et al.*, 2005). Low-Ca boninite (star) represents primitive matrix glass from Cape Vogel (Papua New Guinea) from Kamenetsky *et al.* (2002).

represent an important component within the magmatic system from which the olivines crystallized, rather than fractions of exotic and ephemeral melt that was trapped accidentally. However, the nepheline-normative inclusions in the LC and transitional olivine crystals do not conform to this general pattern. They generally have low SiO_2 contents (<45 wt %) and sometimes have larnite or kalsilite in the norm; they all have higher CaO/Al_2O_3 ratios (0·6–1) than the hypersthene-normative inclusions, reflecting higher calcium contents.

For assemblages dominated by clinopyroxene–olivine fractionation, the CaO/Al_2O_3 ratio can be used as an index of fractionation. As this ratio also distinguishes between LC and HC olivine-hosted inclusions, it has been used as the *x*-axis in Fig. 8. For HC olivines, K_2O and Na_2O contents increase with decreasing

CaO/Al_2O_3 ratio, but the hypersthene-normative inclusions in LC olivine crystals do not fall on this trend, as their range in potassium and sodium contents ranges to lower values than expected from the extrapolation of the HC trend. Contents of TiO_2 and P_2O_5 are scattered, with the former oxide reaching lower average levels in the inclusions within LC olivine and the latter higher concentrations. No obvious systematic differences can be seen in S or F concentrations, although both elements are higher in LC-olivine-hosted nepheline-normative (LC-Ne) inclusions. Most of the inclusions in HC olivine do not reach more than 0·32 wt % Cl, but this element can be as high as 0·7 wt % in hy-normative inclusions within LC and LC-HC olivine. The inclusions with high Cl contents have somewhat lower electron microprobe totals, which may indicate that these glasses are rich in H_2O. They also have lower K/Cl ratios (<15) than the HC-olivine-hosted inclusions (10–34). These Cl contents are higher than for nearly all other subduction-related glasses, for which Cl contents normally range between 0·1 and 0·5 wt % (Harris & Anderson, 1984; Sisson & Layne, 1993; Gioncada *et al.*, 1998; Sisson & Bronto, 1998; Luhr, 2001; Kent & Elliott, 2002; Cervantes & Wallace, 2003; Stix *et al.*, 2003; Métrich *et al.*, 2004), apart from some unusually halogen-rich glasses from the Izu volcanic front with up to 0·8 wt % Cl (Straub & Layne, 2003). Fluorine contents are also high compared with the global arc literature (typically <0·1 wt %), although data are scarcer than for Cl. The inclusions from LC olivine 2009 have a lower Cl (0·22 wt %) content than the other hypersthene-normative inclusions, apart from the melts next to the orthopyroxene within LC olivine, which show an even more pronounced depletion in this element (Fig. 8). The glass rims next to orthopyroxene inclusions are also more silicic than the other hypersthene-normative glass inclusions, but their composition is similar in other respects.

Modelling of FeO-diffusion profiles

FeO contents for most melt inclusions were lower than expected for melts in equilibrium with high-forsterite olivine. This probably reflects FeO loss, resulting from re-equilibration with the enclosing olivine (Danyushevsky *et al.*, 2000). This process has major effects on the FeO and MgO concentrations of melt inclusions, and can thereby also change the absolute concentrations of other elements. It is therefore important to try to undo the effect of this re-equilibration process. This can in principle be done by modelling the FeO profiles around the inclusions, following the technique described by Danyushevsky *et al.* (2002). This is an elaborate process, where the FeO profile in the olivine is modelled as a function of the (known) size of the inclusion, the initial temperature of trapping (approximated by homogenization temperature of the glass), the unknown initial FeO content of the melt inclusion, and the unknown cooling interval and duration of cooling before eruption. The three unknowns in this model are then adjusted until the modelled FeO profile of the olivine and the modelled composition of the melt inclusion match the measured profile and melt inclusion composition.

FeO profiles in olivine were measured around a number of HC- and LC-olivine-hosted melt inclusions. For all HC olivines, FeO contents increased towards inclusions, whereas this type of zoning was less pronounced near inclusions within LC olivine. This zoning is superimposed upon any zoning seen in the olivine crystal as a whole. The modelling focused on the inclusions in the HC olivine crystals, because their initial FeO* concentration was likely to be similar to that of the whole-rock (9 wt %) or other mafic whole-rock samples of the series (9·7–10 wt %), providing a likely starting composition of the melt inclusion. However, we failed to produce a match for both the FeO profiles and the measured melt inclusion composition using ≥9 wt % FeO* as the original concentration of the melt inclusions in HC olivines. The profiles could be reproduced only if initial FeO* contents of the melt were taken to be as low as 6–7 wt % (Table 4, Fig. 9). This is lower than expected for a melt in equilibrium with these olivines, and also significantly lower than the whole-rock FeO* content of the host rock, or any other mafic sample from the series. This probably signifies that the inclusions have undergone more than one period of equilibration and Fe loss, and that the profile measured around the inclusion represents only the last equilibration event. The duration of this last equilibration event varied from 4 to 194 days, but no systematic variation of the duration with the forsterite content of the enclosing olivine was observed. The temperature of last equilibration varied between 925 and 1120°C, and showed a negative correlation with the duration of the last equilibration event.

When the FeO profiles were measured around melt inclusions, it was observed that CaO contents in olivine increased and NiO content decreased towards the melt inclusion (Fig. 10). This was especially noticeable for the inclusions in the LC olivine crystals. This increase in measured CaO content in olivine next to a phase with higher CaO concentrations is sometimes ascribed to secondary fluorescence of the high-Ca phase. However, the anti-correlation of CaO and NiO in the profile, and the fact that Al_2O_3 concentrations do not show an apparent elevation, argues against secondary fluorescence being the main reason for this CaO increase. We think that post-entrapment equilibration between olivine and the included glass phase also explains the CaO

Table 4: Results of modelling of the FeO profile in olivine around the melt inclusion

Sample:	ol24-4	ol31-3	ol13-8	ol13-9	ol117-2	ol35-1	ol77-9
Type:	HC-HF	HC-HF	HC	HC	HC	HC-LF	HC-LF
mg-no. ol:	91·65	91·31	88·32	88·34	87·97	84·24	85·17
NiO ol:	0·25	0·21	0·21	0·20	0·20	0·19	0·20
CaO ol:	0·36	0·43	0·45	0·45	0·41	0·42	0·40
Fe^{2+}/Fe^{3+}:	5·0	5·0	6·0	6·0	3·5	3·0	3·0
Start melting:	1020	1020	946	946	915	884	878
T last daughter:	1183	1250	1192	1192	1193	1114	1191
T quench:	1260	1291	1226	1226	1235	1222	1196
mg-no. ol:	92	91	88	88	88	84	85
Dry melts (normalized to 100 wt %)							
SiO_2 glass	48·43	48·16	48·91	49·49	47·59	50·59	50·05
TiO_2 glass	0·80	0·72	1·07	1·03	0·92	0·75	0·72
Al_2O_3 glass	14·70	14·19	15·14	14·67	16·59	17·11	16·73
FeO glass	4·78	4·69	5·57	5·82	5·19	5·64	5·77
MnO glass	0·07	0·06	0·10	0·07	0·09	0·09	0·12
MgO glass	10·24	10·96	7·97	7·53	8·69	7·12	6·49
CaO glass	14·43	15·30	13·47	14·11	13·20	10·39	11·80
Na_2O glass	2·24	2·23	2·16	2·10	2·31	2·65	2·77
K_2O glass	3·56	3·28	5·13	4·73	4·74	5·16	4·96
P_2O_5 glass	0·77	0·42	0·48	0·45	0·67	0·49	0·61
Calculated melts to FeO = 9·00 wt %							
SiO_2	46·71	46·54	47·53	48·02	46·48	49·39	48·83
TiO_2	0·7	0·64	0·97	0·92	0·88	0·71	0·67
Al_2O_3	12·78	12·56	13·74	13·16	15·79	16·23	15·71
Fe_2O_3	1·67	1·67	1·43	1·43	2·5	2·52	2·49
FeO	7·5	7·52	7·73	7·75	6·76	6·8	6·73
FeO*	9·0	9·0	9·0	9·0	9·0	9·1	9·0
MnO	0·06	0·05	0·09	0·06	0·09	0·09	0·11
MgO	12·33	12·22	9·23	9·45	7·62	6·54	6·54
CaO	12·55	13·54	12·22	12·66	12·55	9·85	11·08
Na_2O	1·95	1·98	1·96	1·89	2·19	2·52	2·6
K_2O	3·09	2·9	4·66	4·25	4·51	4·9	4·65
P_2O_5	0·67	0·37	0·44	0·4	0·64	0·46	0·57
T_{calc}	1329	1326	1267	1266	1211	1201	1190
Fo_{calc}	91·35	91·39	88·5	88·59	87·7	85·44	85·61
Ol%	11·87	10·01	8·08	9·33	3·04	3·53	4·62
Initial melt used for modelling							
FeO* in melt	7·00	6·00	6·00	6·00	6·00	6·00	6·00
SiO_2	47·78	48·10	49·03	49·61	47·76	50·97	50·29
TiO_2	0·78	0·75	1·10	1·06	0·98	0·79	0·75
Al_2O_3	14·3	14·75	15·65	15·02	17·65	18·08	17·43
Fe_2O_3	1·3	1·12	0·95	0·95	1·47	1·65	1·66
FeO	5·83	5·03	5·12	5·13	4·63	4·46	4·48
MnO	0·07	0·06	0·10	0·07	0·10	0·1	0·13
MgO	9·52	8·12	6·08	6·25	5·16	4·21	4·3
CaO	14·04	15·90	13·92	14·45	14·04	10·97	12·29
Na_2O	2·18	2·32	2·23	2·15	2·45	2·8	2·89
K_2O	3·46	3·41	5·30	4·85	5·04	5·45	5·16
P_2O_5	0·75	0·43	0·50	0·46	0·72	0·52	0·63
T_{calc}	1259	1212	1162	1161	1117	1107	1096

Table 4: Continued

Sample:	ol24-4	ol31-3	ol13-8	ol13-9	ol117-2	ol35-1	ol77-9
Type:	HC-HF	HC-HF	HC	HC	HC	HC-LF	HC-LF
mg-no. ol:	91·65	91·31	88·32	88·34	87·97	84·24	85·17
NiO ol:	0·25	0·21	0·21	0·20	0·20	0·19	0·20
CaO ol:	0·36	0·43	0·45	0·45	0·41	0·42	0·40
Fe^{2+}/Fe^{3+}:	5·0	5·0	6·0	6·0	3·5	3·0	3·0
Start melting:	1020	1020	946	946	915	884	878
T last daughter:	1183	1250	1192	1192	1193	1114	1191
T quench:	1260	1291	1226	1226	1235	1222	1196
mg-no. ol:	92	91	88	88	88	84	85
Modelled melts after re-equilibration and experiments							
SiO_2	48·28	48·09	48·73	49·55	47·48	50·50	49·92
TiO_2	0·80	0·72	1·06	1·04	0·92	0·75	0·72
Al_2O_3	14·61	14·17	15·03	14·76	16·60	17·07	16·69
FeO*	4·81	4·52	5·76	5·29	5·18	5·75	5·69
MnO	0·07	0·06	0·10	0·07	0·09	0·09	0·12
MgO	10·33	11·02	8·02	7·55	8·56	7·12	6·52
CaO	14·34	15·28	13·38	14·21	13·20	10·19	11·77
Na_2O	2·23	2·23	2·14	2·11	2·30	2·64	2·77
K_2O	3·53	3·28	5·09	4·77	4·74	5·15	4·94
P_2O_5	0·77	0·41	0·48	0·44	0·68	0·49	0·60
Re-equilibration conditions							
Cooling interval (°C)	230	170	40	80	190	95	70
T re-equilibration (°C)	1029	1040	1120	1080	925	1013	1024
% of re-equilibration	87	95	80	80	82	80	85
Time (days) of re-equilibration	195	62	4	4	194	74	22

All models were started with the recalculated melt inclusion composition assuming FeO* = 9% wt %. Start melting is the temperature (°C) at which the first melt formed within the melt inclusion during the reheating experiment. *T* last daughter is the temperature (°C) at which the last daughter mineral disappeared during the reheating experiment. *T* quench is the temperature (°C) at which the reheating experiment was quenched. $Fe^{2+}/Fe^{3+} = Fe^{2+}/Fe^{3+}$ ratio of the melt inclusion, based on the Fe^{2+}/Fe^{3+} ratio of spinel. FeO* is total Fe as FeO. Ol% is wt % of olivine crystallized on the wall of the melt inclusion during cooling. T_{calc} is the calculated liquidus temperature for melt inclusion. Fo_{calc} is the calculated forsterite content of olivine in equilibrium with melt inclusion. *T* re-equilibration is the temperature (°C) at which the melt inclusion re-equilibrated with the enclosing olivine.

enrichment of the olivine around the melt inclusion, analogous to the observed FeO enrichment.

Correction for FeO loss

As the original FeO content of the melt inclusions could not be retrieved by modelling the diffusion profile around the inclusions, the true initial FeO content of the melt could not be determined accurately. The inclusions were therefore recalculated using different initial FeO contents, varying between 9·5 and 6·5 wt % for the inclusions within HC olivine (i.e. varying between values for whole-rocks, and those obtained from the modelling), and between 4 and 7 wt % for inclusions in LC olivines (as Fe values were on average lower, and Fe loss appeared to be less pronounced in these inclusions). The maximum discrepancy observed between the measured value and a corrected value was 8 rel. % for SiO_2, and up to 23 rel. % for TiO_2, Al_2O_3, CaO, Na_2O, K_2O and P_2O_5, when a melt inclusions with a measured FeO content of 2·5 wt % was corrected to 7 wt %. Most corrections were, however, significantly smaller. To give an impression of the effect of the corrections, Fig. 11 shows selected Harker variation diagrams for the uncorrected data, the data corrected to a 'best guess' FeO content, and the data corrected to 7 wt % FeO. The best guess amounted to 9·5 wt % FeO for the inclusions in HC-LF and transitional HC olivines; 9 wt % FeO for the inclusions in the HC-HF olivines; 4·0 wt % FeO for the Hy-normative inclusions in LC olivine; 4·8 wt % FeO* for the Ne-normative LC-olivine hosted inclusions; and variable FeO contents between

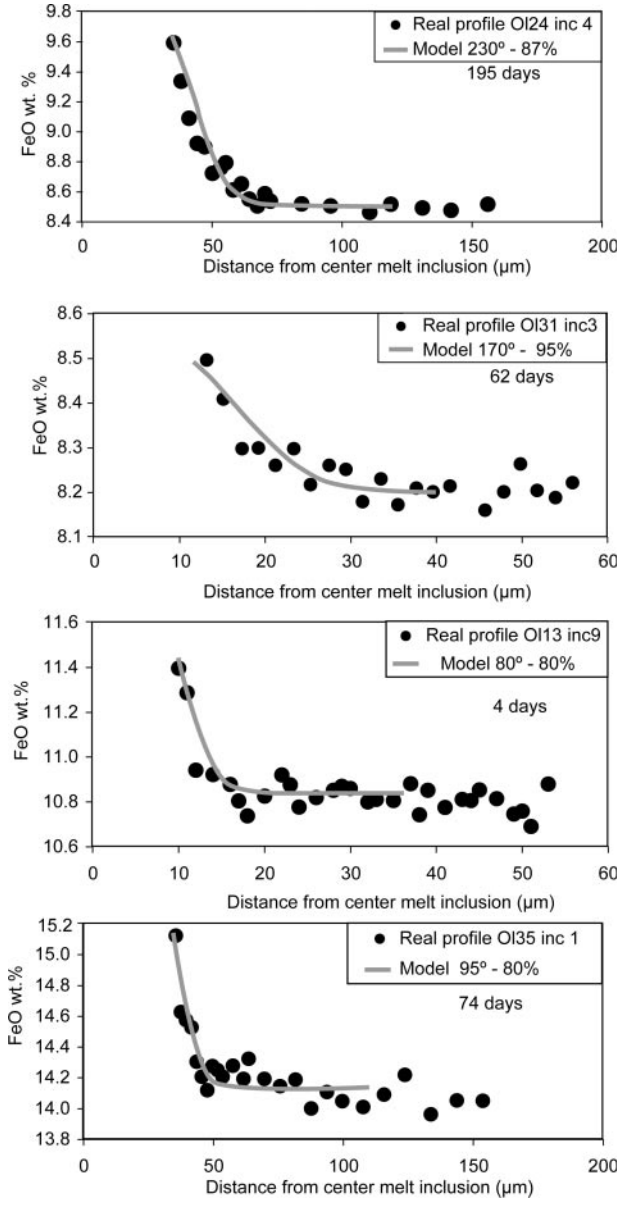

Fig. 9. FeO (wt %) profiles in HC olivines with distance from the centre of the melt inclusion. Circles indicate measured values, grey curves denote models following Danyushevsky *et al.* (2002); cooling interval, percentage equilibration and time period of equilibration are indicated on the diagrams. The compositions of the melt inclusions before and after equilibration are given in Table 4.

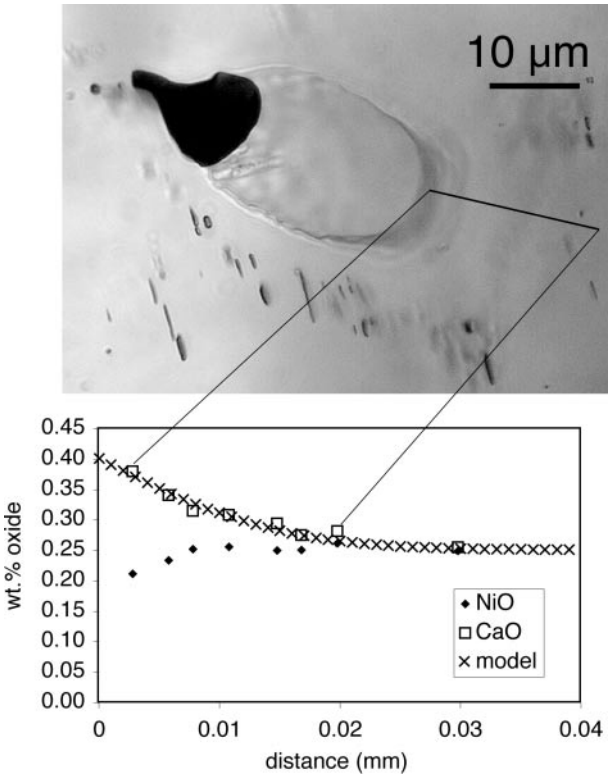

Fig. 10. Transmitted light microscopy image of melt inclusion 2 in an LC-HC olivine (sample 99), showing enrichment of CaO and depletion of NiO in the olivine close to the inclusion. The antithetic behaviour of these two elements, and the fact that alumina does not show significant enrichment in the analyses closest to the inclusion, indicates that the CaO enrichment is not caused by secondary fluorescence. FeO contents of the olivine decrease from 12·3 to 12·1 wt % in the same traverse with distance from the inclusion. The crosses indicate the modelling of CaO loss to the olivine (Appendix), and suggest that this small inclusion, with measured CaO contents of 4·5 wt %, originally contained 5·2 wt % CaO if the measured increase of CaO in the olivine next to the inclusion was a result of CaO diffusion from the inclusion into the olivine.

4·4 and 7 wt % for the inclusions in transitional HC-LC olivines.

An important result of the systematic assessment of the FeO loss correction was that this correction did not affect the silica saturation of the inclusions: inclusions within HC olivines remained silica-undersaturated irrespective of assumed FeO* content (olivine, nepheline with or without leucite in the norm); hypersthene-normative inclusions within LC olivines remained hy-normative, and ne-normative inclusions within LC olivines remained ne-normative.

The FeO correction does, of course, change the FeO and MgO content of the inclusions significantly. As the values for these oxides are a direct reflection of the correction, they can no longer give us any relevant geological information, and have therefore not been used. As we cannot be sure that our assumed FeO contents are correct, we prefer to use the uncorrected data for further discussion. The CaO/Al_2O_3 ratio was used as a fractionation index in Fig. 8; the variation of this ratio with the recalculated SiO_2 content is given in Fig. 11.

Trace elements and water

Trace element data, normalized to normal mid-ocean ridge basalt (N-MORB; Sun & McDonough, 1989)

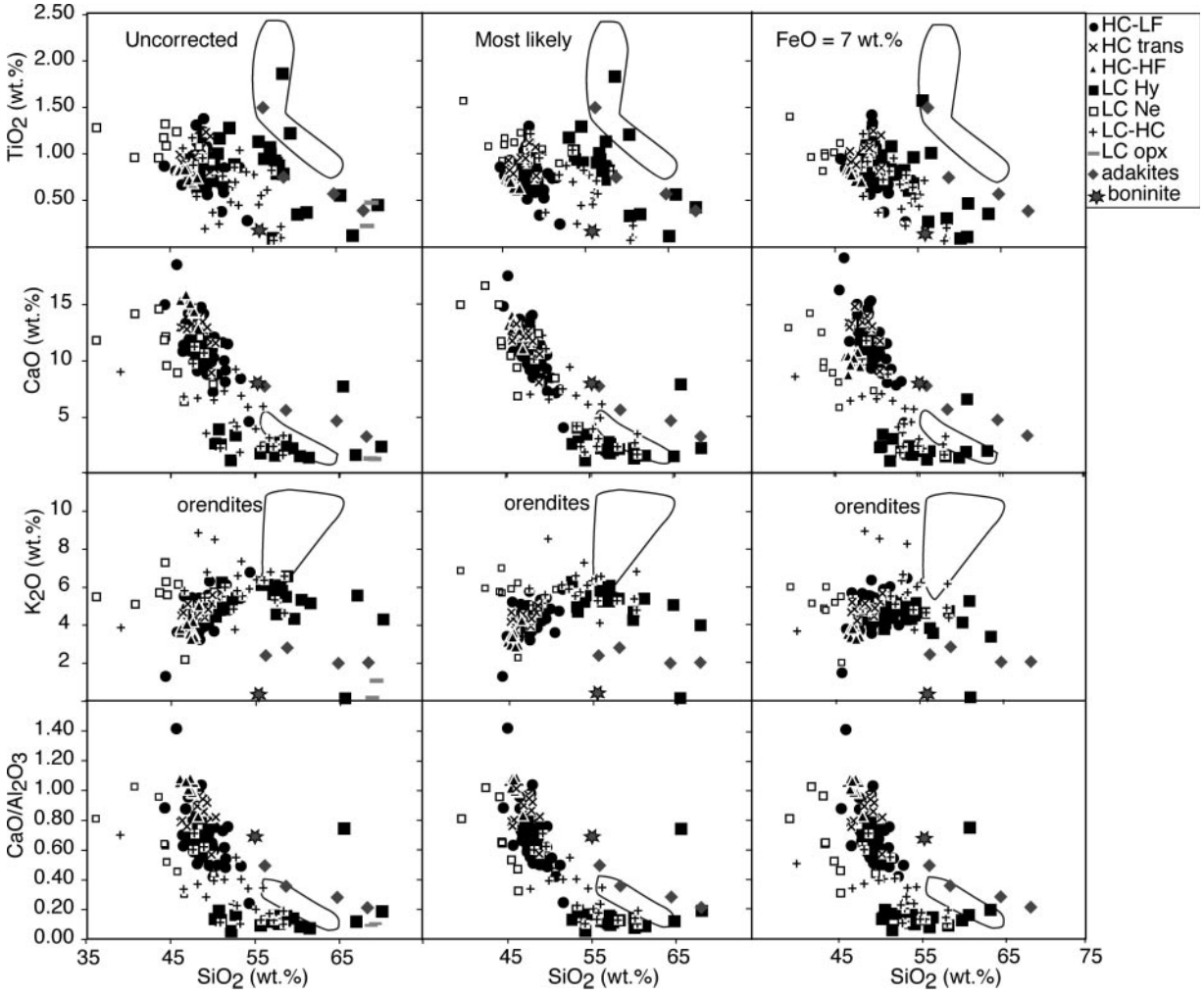

Fig. 11. Melt inclusion composition data for selected oxides and ratios against SiO_2 content (wt %). The first column shows the uncorrected data; the second column shows the data corrected to the most likely FeO* contents (4–9·5 wt %; see text); the third column shows all data corrected to 7 wt % FeO*. Data for orendites, adakites and boninite as in Fig. 8.

are shown in Fig. 12. Melt inclusions from LC and HC olivines have similar patterns for all elements except for the heavy REE (HREE) and Y (Figs 12–14). All melt inclusions show the hallmarks of subduction-related magmas, with strong enrichments in the large ion lithophile elements (LILE), such as Rb, Ba and Sr, and relative depletions for the high field strength elements (HFSE), such as Nb, Ta and Ti. The inclusions from LC and LC-HC olivine crystals generally have higher contents of LILE and LREE than the HC-olivine-hosted inclusions (Fig. 13). The former show much lower contents of Y and the HREE (Table 1), leading to Gd/Yb and Sr/Y ratios well in excess of those for the inclusions in HC olivine or for MORB. There is a good correlation between Zr, Th, the LILE and HREE (Fig. 13). No correlation is seen between trace element concentrations and the forsterite content of the olivine in which these inclusions occur.

The rare earth element pattern of an orthopyroxene (opx b) included in an LC olivine shows a somewhat HREE-depleted pattern, at very low absolute levels of REE (Fig. 14). When orthopyroxene–melt distribution coefficients from McKenzie & O'Nions (1991) are used to calculate the REE pattern of the melt in equilibrium with this orthopyroxene, the result shows a clear resemblance to the melt inclusions in LC olivine crystals, with LREE enrichment and HREE depletion. The pattern shows some spikes and troughs, which are interpreted to reflect inaccuracy in the measurements of these elements in the orthopyroxene because of very low concentrations (0·3–0·02 times chondrite).

Ion microprobe measurements for H_2O, Li and B were made late in the study, when few inclusions of

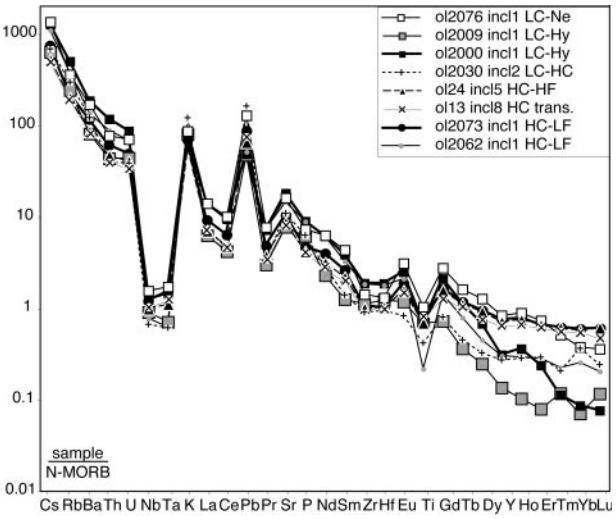

Fig. 12. N-MORB-normalized trace element patterns for representative inclusions of the different groups, showing strong similarities in the most incompatible element ratios. The hypersthene-normative LC inclusions show strong HREE depletion.

sufficient size and quality were left for analysis. Therefore, only one Hy-normative inclusion in LC olivine was analysed (from olivine 2009), which did not have high Cl contents. Water contents in the 10 analysed inclusions varied between 0·56 and 0·94 wt %, and show a correlation with the K_2O content of the glass (Table 5), but without any distinctions between the groups (as far as can be seen in this limited dataset). We are not completely convinced that these values represent primary water concentration of the magmas. The decrepitation marks around some inclusions indicate that volatiles may have been lost, and recent experiments have shown that water loss by proton diffusion through olivine enclosed in magmas that have been affected by degassing can happen in a matter of hours (Hauri, 2002).

Lithium contents in the inclusions in which H_2O was measured varied between 7 and 20 ppm, with one outlier in an HC-LF-olivine-hosted inclusion at 33 ppm. Apart for the analysed LC-olivine-hosted inclusion, a correlation seems to exist between Na_2O and Li contents of the inclusions (Table 5). Boron contents vary between 17 and 52 ppm, and a correlation exists between B and the Fo content of the enclosing olivine, with the LC-olivine-hosted inclusion having the highest B content. B and Li contents were also measured in the host olivine of one of the HC-HF group and the LC olivine, yielding olivine–liquid distributions coefficients for Li of 0·4 and 0·27, and for B of 0·009 and 0·018. These values are slightly higher than but within the same order of magnitude as the values reported by Zanetti *et al.* (2004) for a hydrous basanite melt (0·22 and 0·0058 for Li and B, respectively).

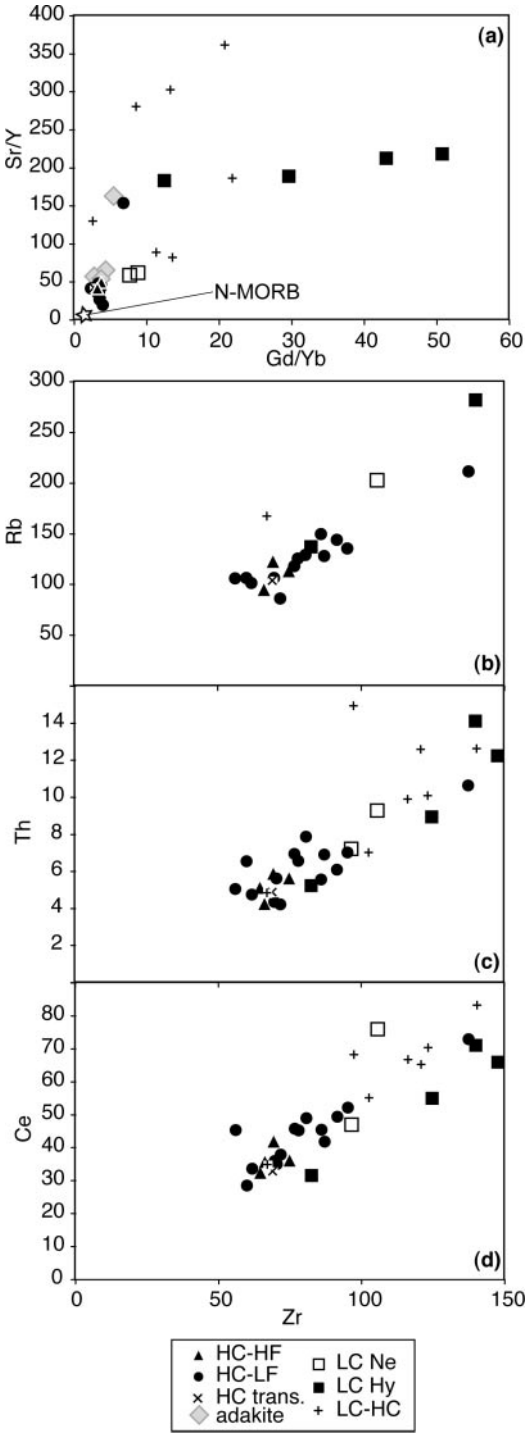

Fig. 13. (a) Sr/Y vs Gd/Yb for the glass inclusions. All true HC inclusions have low Gd/Yb ratios, but higher ratios are seen in the inclusions with higher Sr/Y, with garnet being the most likely phase causing this HREE depletion. Five-pointed star represents average N-MORB (Sun & McDonough, 1989); adakite data are from Martin *et al.* (2005). (b–d) Rb (ppm), Th (ppm) and Ce (ppm) vs Zr (ppm) for the glass inclusions, showing the distinctions between groups and the generally good correlation between these elements with contrasting geochemical behaviour.

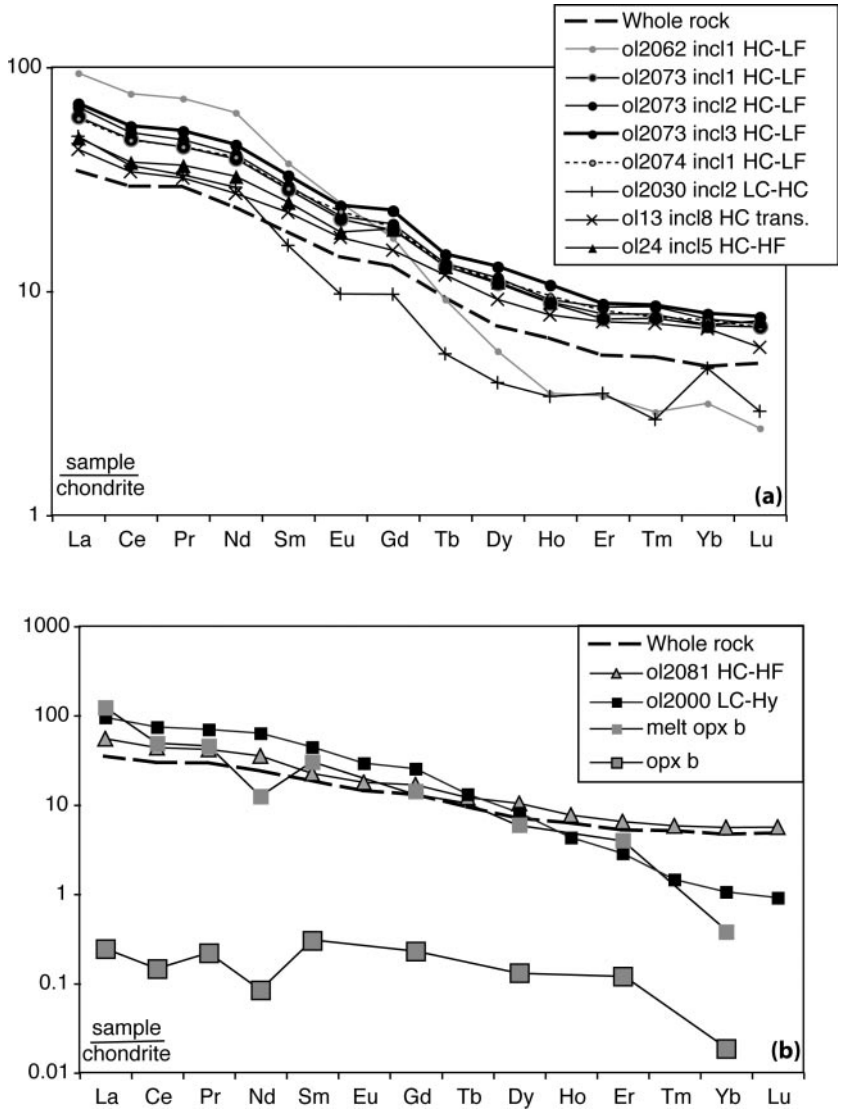

Fig. 14. (a) Chondrite-normalized REE patterns for various inclusions, as measured by LA–ICP–MS. Pattern of whole-rock is shown for reference (Elburg & Foden, 1999). Normalizing values from Evensen *et al.* (1978). (b) Chondrite-normalized REE patterns [note difference in scale compared with (a)] of one of the enclosed orthopyroxenes (spikiness of pattern is an artefact resulting from the very low intensity of the beam), measured by SIMS, and the calculated melt with which it should be in equilibrium. The resemblance to measured pattern for LC melt inclusion should be noted. Pattern for whole-rock and HC-HF melt inclusion are shown for reference.

DISCUSSION

Identification of contrasting magmas

Inclusion relationships have shown that the following phases occur together, and are therefore likely to be genetically related:

(1) HC-LF olivine; high-Ti spinel; clinopyroxene
(2) HC-HF olivine; medium-Ti spinel;
(3) LC olivine; low-Ti spinel; orthopyroxene.

It is unclear whether HC-HF olivine crystals are in equilibrium with clinopyroxene; the fact that no clinopyroxene inclusions were found in HC-HF olivine is possibly a reflection of the scarcity of these olivine crystals. The most magnesium-rich clinopyroxene crystals are also not found in any mutual inclusion relationship; we think it plausible that they were in equilibrium with the HC-HF olivine crystals.

The measured CaO and NiO contents of both the LC and HC olivine crystals are unusual when compared with olivine crystals from 'normal' arc volcanic rocks, which generally have 0·15–0·28 wt % CaO and 0·15–0·40 wt % NiO at $Fo_{86–88}$ [Elburg, unpublished data for North Sulawesi and Alor (Indonesia), Ambryn and Yasur

Table 5: *Melt inclusion and olivine electron microprobe and ion microprobe analyses for H_2O, Li and B*

Sample:	24-5	2009-7	2081-1	2061	2064-1	2052-1	2092	2075	2068	2057a
Group:	HC-HF	LC-Hy	HC-HF	HC-LC	HC	HC-LF	HC-LF	HC-LF	LC-HC	HC-LF
Glass										
SiO_2	47·67	57·85	48·36	56·05	47·65	50·05	48·72	49·95	52·84	47·25
TiO_2	0·88	0·90	0·73	0·54	0·87	0·75	0·84	0·90	0·85	0·91
Al_2O_3	14·81	19·55	15·65	17·24	14·66	17·30	16·30	17·33	16·88	16·60
FeO	4·78	2·34	4·01	3·64	5·52	5·29	5·69	4·84	4·11	6·65
MnO	0·08	0·02	0·10	0·05	0·07	0·09	0·08	0·10	0·05	0·14
MgO	9·66	4·52	8·33	5·83	8·94	7·52	7·56	6·58	6·98	7·49
CaO	14·60	2·51	12·87	5·90	14·71	7·25	11·71	11·01	9·20	13·00
Na_2O	2·22	3·46	2·35	3·43	2·38	2·78	2·62	2·73	2·81	2·81
K_2O	4·17	5·61	5·00	6·32	4·14	3·69	5·06	5·21	5·77	3·91
P_2O_5	0·49	0·81	0·42	0·56	0·47	0·46	0·69	0·57	0·64	0·40
F	0·07	0·12	0·05	0·11	0·09	0·09	0·11	0·08	0·10	0·11
S	0·08	0·01	0·02	0·02	0·06	0·01	0·06	0·05	0·02	0·10
Cl	0·17	0·23	0·23	0·22	0·19	0·16	0·16	0·21	0·15	0·19
Total	99·55	97·83	98·05	99·81	99·67	95·37	99·51	99·49	100·34	99·45
mg-no.	78·3	77·5	78·7	74·0	74·3	71·7	70·3	70·8	75·2	66·7
CaO/Al_2O_3	0·99	0·13	0·82	0·34	1·00	0·42	0·72	0·64	0·55	0·78
H_2O	0·58	0·79	0·66	0·94	0·74	0·56	0·87	0·74	0·79	0·56
Li	7·62	12·96	7·44	32·79	8·64	17·87	16·43	19·57	16·51	17·07
B	44·52	52·82	34·79	33·12	25·88	28·06	25·70	29·35	31·99	17·26
Olivine										
SiO_2	41·26	41·79	40·78	40·03	40·07	40·06	40·07	40·90	41·07	39·54
Al_2O_3	0·04	0·03	0·04	0·03	0·02	0·03	0·03	0·03	0·03	0·04
FeO	8·79	7·32	9·00	12·70	10·34	13·16	12·78	12·53	11·53	13·71
MnO	0·16	0·12	0·20	0·24	0·18	0·24	0·27	0·24	0·21	0·27
MgO	50·11	52·31	49·35	46·28	47·64	45·86	46·30	47·21	48·00	45·09
CaO	0·45	0·20	0·41	0·32	0·56	0·33	0·50	0·41	0·38	0·50
NiO	0·24	0·37	0·23	0·25	0·20	0·20	0·21	0·22	0·27	0·19
Total	101·08	102·17	100·02	99·85	99·02	99·89	100·16	101·53	101·50	99·33
Fo (%)	91·0	92·7	90·7	86·7	89·2	86·1	86·6	87·0	88·1	85·4
Li		3·53	2·96							
B		0·93	0·32							

Oxides in wt %, elements in ppm.

(Vanuatu), Santorini (Greece); Nakamura, 1995; Clynne & Borg, 1997; Tamura *et al.*, 2000; Reubi *et al.*, 2002; Smith & Leeman, 2005]. The HC olivine crystals have high CaO and low NiO contents compared with normal arc volcanic rocks, and, conversely, LC olivine has lower CaO and higher NiO contents. The smooth variations of CaO, NiO and forsterite contents within the HC group as a whole appear to suggest that they belong to a single fractionation series, and we propose that they co-crystallized with clinopyroxene and high-Ti spinel. This apparent fractionation series (see discussion below) accounts for the majority of phenocrysts within the sample. The melt inclusions in the HC olivine crystals are also closer to the whole-rock composition than those in LC olivine, and this suggests that the whole-rock composition (Tnv11, Table 1) is dominated by the contribution from HC melt and crystals.

If the HC-HF and HC-LF olivine crystals are members of a single fractionation series, then LC olivine cannot belong to this fractionation series, since LC olivine has far higher NiO and lower CaO contents at similar forsterite contents than HC olivine. Moreover, pyroxene enclosed within LC olivine is always orthopyroxene rather than clinopyroxene. It is therefore unlikely

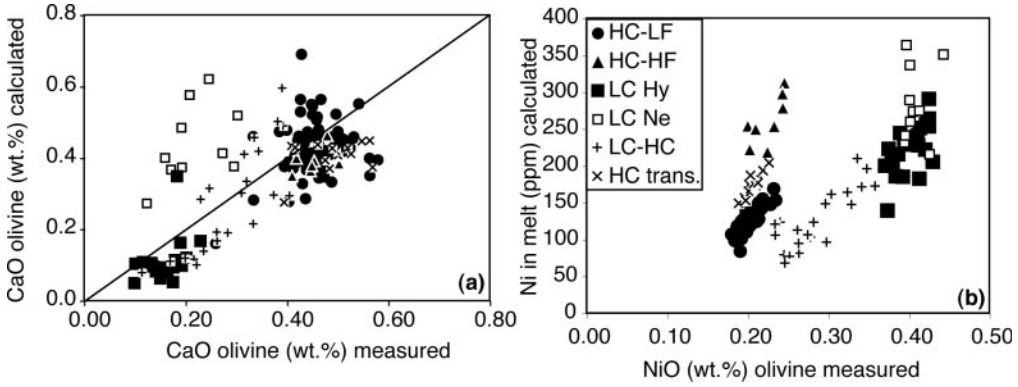

Fig. 15. (a) Calculated vs measured CaO content (wt %) of olivine, using the K_d calculation of Beattie *et al.* (1991) for FeO-corrected melt inclusion compositions. Line of 1:1 correlation is for reference only. The match is generally good, apart for the Ne-normative LC inclusions. The calculated contents of the Hy-normative inclusions are slightly low because of Ca loss of the inclusion to the olivine (see Appendix). (b) Calculated Ni content of the melt vs NiO content (wt %) of olivine. The Ne-normative LC inclusions give very high calculated Ni contents, but the fact that these inclusions do not appear to be in Ca equilibrium with the olivine host casts a severe doubt on this result. Despite the higher NiO content of the LC olivine crystals, calculated Ni contents of the melt are similar to the Ni contents of the most primitive HC melts.

that LC olivine crystals were in equilibrium with the same magmas from which the HC phenocrysts formed.

Ca and Ni in olivine and melt inclusions: origin of Ne-normative LC inclusions

With respect to their low CaO and high NiO and MgO contents, LC olivine crystals resemble olivine from mantle xenoliths and peridotites (Dick, 1989; Pearce *et al.*, 2000; Griselin, 2001; McInnes *et al.*, 2001), even though the latter seldom exceeds 93 mol % Fo and 0·4 wt % NiO. Forsterite-rich low-Ca olivine crystals within volcanic rocks are often interpreted as mantle xenocrysts (Ramsay *et al.*, 1984; Cameron, 1985; Boudier, 1991; Rohrbach *et al.*, 2005); however, we suggest that the LC olivine crystallized from a melt and is not a mantle-derived xenocryst (Kamenetsky *et al.*, 2006).

A strong argument for the magmatic interpretation is the coherence between the CaO content of the melt inclusions and their enclosing olivines. Using the olivine–melt distribution coefficients from Beattie *et al.* (1991), we can calculate the CaO content of the olivine with which the melt inclusions would have been in equilibrium (Fig. 15a). The distribution of calcium between olivine and melt is dependent on the MgO distribution, which is influenced by the FeO* recalculation procedure. The calculation has been performed with the 'best guess' FeO* recalculation, but the trends are similar if the raw data are used. The calculated olivine CaO contents correspond reasonably well to the measured CaO contents of the enclosing olivine. An exception is formed by the LC-olivine-hosted nepheline-normative melts, which give olivine CaO contents that are significantly higher than the measured concentrations. The generally good match between the calculated and actual CaO contents cannot be a result of later equilibration between olivine and melt, as CaO enrichment of the olivine close ($<15\,\mu m$) to the inclusion (Fig. 10) demonstrates that diffusional equilibration for CaO has been limited, in keeping with the slow diffusion for this element in olivine (Petry *et al.*, 2004). Although CaO concentrations in the olivine around the inclusions are low compared with those in the inclusions (0·4 wt % vs 4 wt %), the small size of the hy-normative inclusions in LC-olivine results in the CaO loss being non-negligible, and it could be as high as 15 rel. % for a typical inclusion with a diameter of $25\,\mu m$ and a measured CaO content of 4 wt % (see the Appendix). This could explain why the calculated CaO contents of the enclosing olivine are generally slightly low for the hypersthene-normative inclusions in LC olivine, whereas no systematic offset is seen for the inclusions in the HC olivines. As the exact amount of CaO loss depends on the initial CaO content of the melt inclusion, its size and the diffusion profile around the inclusion, we did not apply a correction for this effect, as diffusion profiles were not measured around all inclusions.

The CaO contents of the melt inclusions within the olivines support the idea that the HC and Hy-normative LC inclusions could represent the melt from which the olivine crystallized. The NiO contents of the olivine can be used in a manner similar to the CaO content to calculate the Ni concentration of the parental melt. The LC olivine crystals contain significantly more NiO than HC olivine crystals, which could be interpreted as crystallization from a more NiO-rich melt. However, if we assume that the parental melt had a bulk composition similar to that of the melt inclusions (again corrected for FeO* loss), then the different melt structure between the

inclusions in the two major groups of olivines would cause a significant difference in the Ni olivine–melt distribution coefficient. This compositional effect is far more pronounced for Ni than it is for Ca. Therefore, calculated Ni contents in the melts parental to LC and HC-HF olivine would not differ much, ranging between 200 and 300 ppm (Fig. 15b). If uncorrected melt inclusion compositions are used, the calculated Ni values for both groups lie between 100 and 200 ppm. Three of the Ne-normative glasses in LC olivine have higher calculated Ni contents around 350 ppm. Considering the fact that the Ne-normative inclusions did not appear to be in equilibrium with their host olivine for Ca, these calculated Ni contents are unlikely to be correct. The whole-rock contains significantly more Ni (664 ppm; Elburg & Foden, 1999) than the calculated Ni contents of the melt inclusions. This is likely to reflect olivine accumulation, indicating that this whole-rock compositions cannot be equated with a melt composition.

The calculations suggest that the nepheline-normative melt inclusions in LC olivine are not in equilibrium with their host. The two main options for the formation of these inclusions are that they represent aliquots of HC melt that has been accidentally trapped in LC olivine; or that they do not represent liquid compositions. The first option seems unlikely, as the ne-normative LC inclusions have different Sr/Y and Gd/Yb ratios from true HC melt inclusions (Fig. 13a). We therefore think that the ne-normative melt inclusions in LC olivine represent inclusions from which some melt has escaped after partial crystallization. This would enrich the inclusion in olivine and clinopyroxene components (Portnyagin *et al.*, 2005), whereas silicic liquid would escape. Because clinopyroxene has a higher liquid–solid distribution coefficient for the HREE, this process can also explain the reduced Sr/Y and Gd/Yb ratios compared with the hy-normative inclusions. Phlogopite might also have been a residual phase, causing an enrichment in K_2O and F, whereas the higher sulphur contents could be explained by the formation of iron sulphides.

Distinction between melt inclusions in HC-HF and HC-LF olivine

The smooth variation of CaO and NiO with forsterite contents between HC-HF and HC-LF olivine is suggestive of a single fractionation series, but the very minor depletion in NiO between the two subgroups is surprising, since both clinopyroxene and olivine have high mineral/liquid distribution coefficients for this element [around two for clinopyroxene and 8–18 for olivine, using the formulation from Beattie *et al.* (1991)]. However, olivine–liquid distribution coefficients distribution increase strongly with fractionation, so NiO contents in olivine will decrease far more slowly during fractionation than the Ni content of the liquid with which it is in equilibrium.

More doubt is cast upon the fractionation relationship between the melts in HC-HF and HC-LF olivines by the variation of P_2O_5 vs CaO/Al_2O_3 (as a potential fractionation index) (Fig. 8), where P_2O_5 contents within HC-HF-olivine-hosted inclusions vary between 0·3 and 1·05 wt % at $CaO/Al_2O_3 = 1$, and within HC-LF-olivine-hosted inclusions between 0·44 and 1·03 wt % at $CaO/Al_2O_3 = 0{\cdot}65$ (with 1 S.D. on P_2O_5 analyses 0·02 wt % at the 0·2 wt % level). Absolute levels of P_2O_5 (or any other oxide) are influenced by the FeO correction, but this affects concentrations by less than 25% relative, instead of the 300% observed here. Oxide ratios are not influenced by the FeO recalculation and can therefore be used more reliably to assess fractionation behaviour. A diagram of K_2O/Al_2O_3 vs CaO/Al_2O_3 (Fig. 16) shows that K_2O/Al_2O_3 ratios increase when CaO/Al_2O_3 ratios decrease between HC-HF- and HC-LF-hosted melt inclusions. This general trend would be expected for a fractionating assemblage of olivine ($K_2O/Al_2O_3 = 0$, $CaO/Al_2O_3 = 8$–22) and clinopyroxene ($K_2O/Al_2O_3 = 0$–$0{\cdot}02$, $CaO/Al_2O_3 = 5$–25 at mg-number >84), but the K_2O/Al_2O_3 ratio increases too fast compared with the decrease in CaO/Al_2O_3 for a fractionating olivine–clinopyroxene assemblage. The fractionating assemblage should have a CaO/Al_2O_3 of $<2{\cdot}5$ at $K_2O/Al_2O_3 = 0$, whereas all measured clinopyroxene crystals have $CaO/Al_2O_3 > 3$. Although one could decrease the CaO/Al_2O_3 ratio of the fractionating assemblage by adding spinel, the Al_2O_3 content of spinel in equilibrium with forsterite-rich olivine is only 11–13 wt %, and one would need an unrealistically high percentage of spinel (20–30 wt % of the fractionating assemblage) to fit the K_2O/Al_2O_3 to the CaO/Al_2O_3 ratios for fractionating from HC-HF to intermediate HC compositions.

Simple mixing calculations also show that it is not possible to simultaneously match the (FeO*-corrected) CaO, Al_2O_3, K_2O and SiO_2 concentrations of melt inclusions in HC-HF olivines by adding any combination of analysed clinopyroxene, olivine and spinel to HC-LF olivine-hosted melt inclusions. With these calculations, Al_2O_3 contents are too low and SiO_2 contents too high when CaO and K_2O contents match measured values.

In short, there is too much scatter in oxides such as P_2O_5 and TiO_2 at a given index of fractionation for the melts in the HC olivines to belong to a single simple fractionation series. Moreover, the trends in elemental ratios cannot be explained by fractionation of an assemblage of olivine, clinopyroxene ± Cr-spinel. It is likely that fractionation effects are superimposed upon variations in the mineralogy of the source of the melts.

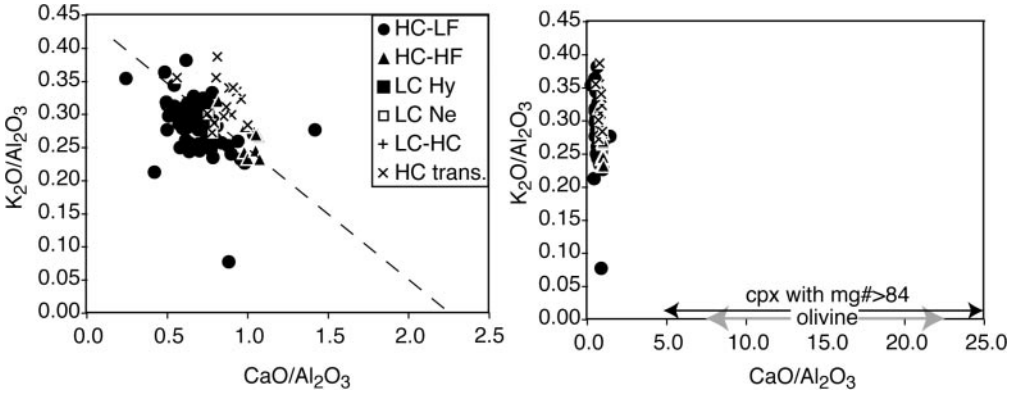

Fig. 16. K_2O/Al_2O_3 vs CaO/Al_2O_3 for HC melt inclusions (uncorrected data, same as corrected data because of normalization to Al_2O_3) and clinopyroxene and olivine crystals. If the HC-LF melts (circles) were formed by removal of crystals from HC-HF melts (triangles), the fractionating assemblage should have $CaO/Al_2O_3 \approx 2{\cdot}5$ at $K_2O/Al_2O_3 = 0$. Measured CaO/Al_2O_3 ratios for clinopyroxene, which should be the main control on CaO/Al_2O_3 variations, vary between 25 (at mg-number 92) and 5 (at mg-number 84) at $K_2O/Al_2O_3 < 0{\cdot}01$. Simple crystal fractionation cannot, therefore, explain the range of HC melts trapped in olivine.

LC melts

Although high CaO/Al_2O_3 melts have been found in many tectonic environments (Schiano *et al.*, 2000; Kogiso & Hirschmann, 2001; Portnyagin *et al.*, 2005), high-silica, low CaO/Al_2O_3 primitive melts are less common. They are either low-Ca boninites, found in hot subduction environments (Crawford *et al.*, 1989), lamproites (Foley *et al.*, 1987) or adakites (Defant & Drummond, 1990). For comparison, Figs 8 and 11 indicate the compositions of representative examples of these magmas. The melt inclusions found in LC olivine crystals cannot be low-Ca boninites, as the latter are characterized by lower Al_2O_3, Na_2O, K_2O and TiO_2 contents (Kamenetsky *et al.*, 2002) than the LC melts. Moreover, HREE depletion is not a characteristic of boninitic melts. Adakitic melts are well known for their HREE depletion, and correspondingly high Sr/Y and Gd/Yb ratios (Martin *et al.*, 2005). However, these melts display lower K_2O, higher Na_2O contents and higher CaO/Al_2O_3 ratios than the LC melt inclusions described here. The closest match to the LC melts in terms of lamproitic rocks is given by orendites from central Italy (Peccerillo *et al.*, 1988), although these contain higher K_2O and less Na_2O than the melt inclusions analysed. Orendites also display HREE depletion, although not as extreme as some of our LC melt inclusions.

The most likely cause of the observed HREE depletion in melt inclusions and orthopyroxenes within LC olivines is equilibration with garnet. Silica-rich melts with low Ca/Al ratios can be formed by crystallization of clinopyroxene, orthopyroxene and garnet from more primitive subduction-related magmas at high pressure and pH_2O (Müntener *et al.*, 2001). However, this process does not agree with the melt inclusions occurring in olivines with extremely high forsterite contents ($\leq Fo_{94}$), as fractional crystallization would rapidly lower the mg-number of the melt. Also, the high forsterite content of enclosing olivine does not favour generation of the liquids by direct melting of the subducted oceanic crust, or by remelting of lower crustal cumulates, unless the magmas or their sources were extremely oxidized and most Fe would occur as Fe^{3+}. Although clinopyroxene can also retain HREE, the middle REE (MREE)/HREE ratios in the LC melt inclusions are too high to be explained by retention in clinopyroxene only (Blundy *et al.*, 1998). The most plausible way to generate the LC-olivine-hosted melt inclusions is by partial melting of a mantle source with residual garnet, or equilibration between melt and a garnet-bearing mantle lithology. If the mantle source started out with HREE contents similar to those of a MORB source, simple batch melt modelling indicates that this source must have contained 20–25 wt % garnet in its residue during partial melting [using the garnet–melt K_d values of McKenzie & O'Nions (1991)]. The presence of garnet in the residue implies either that partial melting took place in a normal peridotitic mantle at depths greater than 90 km, or that the source had a composition that stabilized garnet relative to spinel at lower pressures. A high alumina content, as seen in pyroxenites, is one way of stabilizing garnet (Hirschmann & Stolper, 1996). This agrees with the high Al_2O_3 content of the melt inclusions.

We do not know of any whole-rock analysis that is a perfect match for the LC melt inclusions, but it is possible that the existence of this type of melts is more common than hitherto recognized, as only detailed mineralogical and melt inclusion studies allow us to recognize their existence. Low-Ca olivine is increasingly being reported from subduction settings (Ramsay *et al.*, 1984; Rohrbach *et al.*, 2005), but is commonly interpreted as a mantle xenocryst, and not studied to any

Table 6: Results of MELTS modelling for HC and LC melt inclusions, compared with FeO-corrected melt inclusion analyses*

	HC source	Melt 20 kbar, 1450°C	HC melt inclusion	Residue	LC source	Melt 20 kbar, 1300°C	LC melt inclusion	Residue
SiO_2	50	45·61	45·85	67% cpx	48	52·2	53·74	19% gt
TiO_2	0·5	0·85	0·75		0·5	0·7	0·93	68% cpx
Al_2O_3	8	12·42	12·91		13	19·6	21·04	
FeO	7	11·2	9·5		7	6	4·0	
MgO	15	10·83	11·2		16	6·3	8·6	
CaO	19	14·61	13·97		13	4·7	2·83	
Na_2O	0·8	1·70	1·95		0·8	2·6	2·84	
K_2O	0·6	1·72	3·43		0·6	4·7	4·7	
H_2O	0·3	0·86			0·4	3·1		

Oxides and minerals in wt %.

great extent. We suggest that some characteristics of these low Ca/Al melts stop them from ever reaching the surface. Although the one measured H_2O content was not very high, we failed to analyse inclusions with high Cl contents. It is possible that these have higher water contents, and that the melts reached water saturation before reaching the surface, resulting in degassing and freezing of the melts below the surface, similar to the model proposed by Tamura & Tasumi (2002) for the Izu–Bonin arc.

Similarities and contrasts between LC and HC melts and their sources

The melt inclusions within the LC and HC olivine crystals display very similar trace element patterns, apart from the HREE and Y. They show similar relative depletions in the HFSE and enrichments in the LILE, and in the relative levels of Cs–Rb–Ba enrichment, which are the elements that tend to be variable in arc volcanic rocks, possibly reflecting selective retention in mica or amphibole (Elburg *et al.*, 2002*a*). Also, the good correlation for the dataset as a whole between elements that are thought to be mobile in the fluid phase (such as Rb), and are consequently enriched in arc volcanic rocks relative to MORB, and a fluid-immobile element such as Zr (Fig. 13) suggests that the mantle sources of the LC and HC melts may have had a similar trace element contents.

Despite these similarities, there are significant distinctions between the melt inclusions in LC and HC olivines, with inclusions from LC olivine being calcium poor, silica saturated, chlorine rich and HREE depleted, and those in HC olivine calcium rich and silica undersaturated. HC-olivine-hosted melt inclusions only show a very slight depletion in HREE compared with a MORB source, indicating that garnet is a minor residual phase, if at all. The high CaO contents indicate that the source may have contained significant amounts of clinopyroxene, which entered the melt. Even though the residual mineral assemblages for the LC and HC sources are obviously very different, the similarity in trace element patterns of the melts points towards a close relationship between the sources.

Anomalous source composition

We undertook some exploratory runs with the program MELTS (for pressures <10 kbar) and pMELTS (pressures 10–20 kbar) (Ghiorso *et al.*, 2002) to investigate the possibility of deriving high CaO/Al_2O_3 and low CaO/Al_2O_3 melts from similar sources. Several other workers have attempted to model high CaO/Al_2O_3 melts with the MELTS program (Schiano *et al.*, 2000; Kogiso & Hirschmann, 2001), and found, not unexpectedly, that clinopyroxenite sources give the best results. We obtained the best result with a clinopyroxenite composition that is somewhat more aluminous than the compositions used by other workers (Schiano *et al.*, 2000; Kogiso & Hirschmann, 2001) to model the Ne-normative high CaO/Al_2O_3 melts of the HC olivines (Table 6). If we keep most elements the same, but lower the CaO and increase the Al_2O_3 content of this source, its bulk composition changes from being nepheline-normative to being hypersthene-normative. This then has the desired effect of giving melt compositions that are hypersthene-normative, and leaving a garnet-bearing residue at 20 kbar. This is the smallest change in the source composition that would give the desired effect of obtaining liquids that are very different in terms of major elements. As subduction-zone fluids are thought to be

rich in components derived from the breakdown of aluminosilicates (Manning, 2004), it is feasible that these changes to the mantle are brought about by interaction with this type of fluid.

It is also possible that the distinctions in the LC and HC source's residual mineral assemblage reflect changes in pressure instead of chemical composition. However, an important effect of a pressure increase is to generate melts that are more silica undersaturated (O'Hara, 1968), whereas the LC melts are actually more silica oversaturated than the HC melts. A greater depth of melt generation is therefore unlikely to be the only reason for the presence of garnet in the source.

Because partial melting has the opposite effect on SiO_2 for Hy- and Ne-normative source compositions, the melts of the HC source become lower in silica with decreasing degree of partial melting. To obtain melt compositions with a SiO_2 content around 46–47 wt %, as in the melt inclusions in HC-HF olivines, the (Ne-normative) source needs to be more Si rich than the (Hy-normative) source of the LC melt inclusions (with >50 wt % SiO_2). The degree of melting also needs to be larger than for the LC inclusions, to obtain the desired high Ca/Al ratios. To avoid having to postulate extremely high temperatures, it is most likely that this took place at shallower depth than for the LC inclusions. A similar melt to the one produced at 1450°C and 20 kbar can be produced at 5 kbar at only 1275°C. The larger degree of partial melting leads to rather low K_2O contents in the melt compared with observed values (1·4 vs >3·5 wt %) if the K_2O content of the source is not increased.

As it remains problematic to find a perfect match for this type of liquid by single-stage melting models, it is possible that some of the liquids' geochemical characteristics were obtained during later equilibration with garnet- or clinopyroxene host-rocks. As the equilibrated liquids were still capable of crystallizing Fo_{90} olivine, the equilibration process cannot have involved significant crystallization and must therefore have happened at high temperatures.

Influence of volatile phases

The presence and composition of a volatile phase during partial melting may also have played a role in generating the distinctions between HC and LC liquids. Unfortunately, the pMELTS software can incorporate only H_2O in partial melting models, not CO_2, so we cannot assess this option by computer modelling. It is well known that the presence of water expands the stability field of olivine, and causes the eutectic composition in a water-bearing mantle assemblage to have a relatively high SiO_2 content (Nicholls, 1974), whereas CO_2 has the opposite effect (Mysen & Boettcher, 1975). We notice that LC melt inclusions have higher Cl contents and lower electron microprobe totals than our HC inclusions, and this could point towards a higher dissolved water content in the HC melt component. Alternatively, the high H_2O and SiO_2 contents could both be the result of low degrees of partial melting, rather than the high water content being the cause of the high SiO_2 content. The importance of CO_2 in the magmatic system is evident from our fluid inclusion studies. CO_2-rich fluids have also been proposed as an explanation for high-calcium subduction-related magmatism (Green *et al.*, 2004), although the melts generated in that study were generally hypersthene- instead of nepheline-normative, like our HC melts. The melts produced by Mysen & Boettcher (1975) from a lherzolitic source rock under high-CO_2 conditions were, however, nepheline-normative.

The association of high-Ca melts and water-rich low-Ca melts could also have a bearing on clinopyroxenite–dunite massifs hosting Alaskan- (or Ural)-type Pt deposits, commonly associated with chromitites (Malitch & Thalhammer, 2002). The clinopyroxenite–dunite association indicates a possible genetic relationship to the high-Ca melts associated with the HC olivines. Chromitite segregation, however, appears to be favoured by the presence of a water-rich fluid (Matveev & Ballhaus, 2002), which may point towards a role for a water-rich melt similar to the one associated with the LC olivines. Interestingly, recent work on silicate inclusions within Pt–Fe alloys (Johan, 2006) indicates the presence of low-calcium, high-aluminium ($CaO/Al_2O_3 = 0{\cdot}28$), silicic, water-rich HP melts associated with Uralian–Alaskan-type Pt mineralization.

Preferred model

Whether the coexistence of primitive high-Ca and low-Ca melts is typical for post-subduction magmatism, of which the studied sample is an example, needs further investigation. We envisage a model in which the subducting slab stalls as a result of continental collision, causing an increase in slab temperature with time, as also proposed by Elburg & Foden (1999) for South Sulawesi on the basis of isotope data. This temperature increase could cause the breakdown of hydrous minerals and carbonates that would otherwise have remained stable in the slab at this depth. Water-bearing fluids (or hydrous silicic melts) from the slab would metasomatize the mantle and cause melting. Considering the fact that the presence of water significantly reduces the mantle solidus, and the fact that the mantle near the slab would be warmer than during a normal non-collisional subduction setting, melting took place at relatively high pressures, and in equilibrium with garnet. This would be the source for LC melts. As water would react with the surrounding mantle and become incorporated in melt or water-bearing mineral phases, the remaining fluids

would become enriched in CO_2 (Schuiling, 2004) and continue upwards through the mantle wedge. Melting may then take place at shallower depths in the presence of a CO_2-rich fluid, and generate HC melts. These can continue their upward journey to the surface, but the hydrous LC melts become water saturated at shallower depths and freeze. Therefore, they never erupt, but can only reach the surface if they are carried by their companion HC magma.

CONCLUSIONS

Sample Tnv96-1, on which this mineral and melt inclusion study was performed, is one of several mafic ankaramitic samples within a suite of alkali-rich undersaturated magmas that erupted between 6 and 9 Ma in South Sulawesi. Although their extremely mafic whole-rock compositions reflect cumulate processes, the Sr, Nd and Pb isotopic composition of these samples falls within the range of this suite of samples from South Sulawesi (Elburg & Foden, 1999). The results from the present study can therefore be interpreted to give information on the magma parental to this syn- to post-collisional suite of magmas. The parental magmas are clearly represented by the silica-undersaturated high-Ca suite of melt inclusions, rather than the silica-saturated low-Ca suite. However, the close resemblance in LILE, LREE and HFSE trace element signature between the two types of melt inclusions suggests a genetic relationship between the two melt types, rather than accidental admixture of xenolithic olivine into a high-Ca magma. In light of the good correlation between the composition of the melt inclusion and enclosing olivine, it is unlikely that local melting processes in a cumulate-bearing magma chamber can be blamed for the unusual melt compositions, as suggested by Danyushevsky *et al.* (2004).

The depletion in Y and HREE seen in the high-silica, low-Ca melt inclusions argues for the presence of garnet in the source. The high silica content of these inclusions suggests high water pressure during melt generation. However, the exsolved volatile phase in these inclusions, like that in the high-Ca inclusions, is virtually pure CO_2. This may reflect the lower solubility of CO_2, and thereby enhanced exsolution at lower pressures, in silicate melts, but also loss of H_2O by decrepitation and proton diffusion. It is unavoidable that the latter process has been operational, considering the high diffusivity of hydrogen in olivine and the long storage of these olivines at magmatic temperatures, as shown by the diffusional profiles around the melt inclusions. The high-Ca inclusions have lower silica contents, and are likely to have formed by melting from an H_2O-poor, CO_2-rich source. The fact that many of the most mafic magmas in arc environments show ankaramitic characteristics may reflect the more limited role of degassing-induced fractional crystallization in these H_2O-poor magmas. In contrast, the absence of the high-silica magmas, similar to the low-Ca melt inclusion, as a whole-rock composition within the arc environment may reflect the unavoidable freezing of this magma type because of degassing during ascent and depressurization.

We prefer a model in which the LC and HC melts are formed by melting of normal (non-pyroxenitic) mantle, which was modified by fluids or melts from the stalled subducted slab. These fluids were dominated by H_2O for the LC melts, and by CO_2 for HC melts, which also formed at shallower depths than the LC melts. Whether the coexistence of these two magma types is a local peculiarity or is more common in (post-collisional) subduction environments, and a potential link with Alaskan-type Pt deposits, needs further investigation.

ACKNOWLEDGEMENTS

This research was funded by a European Union Marie Curie Fellowship to the first author. Al Hofmann is thanked for providing the opportunity to pursue this research at the Max Planck Institute for Chemistry in Mainz. The electron microprobe facilities at the Max Planck Institute were financed by a Wolfgang Paul award to A. Sobolev. Stephan Klemme helped with the homogenization experiments in Heidelberg; Ronald Bakker provided access to and help with the Raman spectrometer in Leoben. Andrey Gurenko gave advice on preparation of the melt inclusions, and Nora Groschkopf assisted with electron microprobe analyses. Eric Hellebrand volunteered his help for the ion microprobe analyses, and Brigitte Stoll and Kirsten Herweg helped with the LA–ICP–MS analyses. Igor Nikogosian was supported by ISES (Netherlands Research Centre for Integrated Solid Earth Science). Leonid Danyushevsky is acknowledged for lively discussions and providing the FeO-recalculation program. This paper benefited from thorough reviews by M. Portnyagin and Y. Tamura, and meticulous editorial handling by John Gamble.

SUPPLEMENTARY DATA

Supplementary data for this paper are available at *Journal of Petrology* online.

REFERENCES

Albarède, F. (1995). *Introduction to Geochemical Modelling*. Cambridge: Cambridge University Press, pp. 543.

Bakker, R. J. (2003). Package FLUIDS1. Computer programs for analysis of fluid inclusion data and for modelling bulk fluid properties. *Chemical Geology* **194**, 3–23.

Ballhaus, C., Berry, R. F. & Green, D. H. (1991). High pressure experimental calibration of the olivine–orthopyroxene–spinel oxygen geobarometer: implications for the oxidation state of the upper mantle. *Contributions to Mineralogy and Petrology* **107**, 27–40.

Beattie, P., Ford, C. & Russel, D. (1991). Partition coefficients for olivine–melt and orthopyroxene–melt systems. *Contributions to Mineralogy and Petrology* **109**, 212–224.

Blundy, J. D., Robinson, J. A. C. & Wood, B. J. (1998). Heavy REE are compatible in clinopyroxene on the spinel lherzolite solidus. *Earth and Planetary Science Letters* **160**, 493–504.

Boudier, F. (1991). Olivine xenocrysts in picritic magmas: an experimental and microstructural study. *Contributions to Mineralogy and Petrology* **109**, 114–123.

Burke, E. A. J. (2001). Raman microspectrometry of fluid inclusions. *Lithos* **55**, 139–158.

Cameron, W. E. (1985). Petrology and origin of primitive lavas from the Troodos ophiolite, Cyprus. *Contributions to Mineralogy and Petrology* **89**, 239–255.

Cervantes, P. & Wallace, P. J. (2003). Role of H_2O in subduction-zone magmatism: new insights from melt inclusions in high-Mg basalts from central Mexico. *Geology* **31**, 235–238.

Clynne, M. A. & Borg, L. A. (1997). Olivine and chromian spinel in primitive calc-alkaline and tholeiitic lavas from the southernmost Cascade Range, California: a reflection of relative fertility of the source. *Canadian Mineralogist* **35**, 453–472.

Costa-Rodriguez, F. & Chakraborty, S. (2004). Decadal time gaps between mafic intrusion and silicic eruption obtained from chemical zoning patterns in olivine. *Earth and Planetary Science Letters* **227**, 517–530.

Crawford, A. J., Falloon, T. J. & Green, D. H. (1989). Classification, petrogenesis and tectonic setting of boninites. In: Crawford, A. J. (ed.) *Boninites and Related Rocks*. London: Unwin Hyman, pp. 2–49.

Danyushevsky, L. V., Della-Pasqua, F. N. & Sokolov, S. (2000). Re-equilibration of melt inclusions trapped by magnesian olivine phenocrysts from subduction-related magmas: petrological implications. *Contributions to Mineralogy and Petrology* **138**, 68–83.

Danyushevsky, L. V., Sokolov, S. & Falloon, T. J. (2002). Melt inclusions in olivine phenocrysts: using diffusive re-equilibration to determine the cooling history of a crystal, with implications for the origin of olivine-phyric volcanic rocks. *Journal of Petrology* **43**, 1651–1671.

Danyushevsky, L. V., Leslie, R. A. J., Crawford, A. J. & Durance, P. (2004). Melt inclusions in primitive olivine phenocrysts: the role of localized reaction processes in the origin of anomalous compositions. *Journal of Petrology* **45**, 2531–2553.

Davidson, J. P. (1996). Deciphering mantle and crustal signatures in subduction zone magmatism. In: Bebout, G. E., Scholl, D. W., Kirby, S. H. & Platt, J. P. (eds) *Subduction: Top to Bottom. Geophysical Monograph, American Geophysical Union* **96**, 251–262.

Defant, M. J. & Drummond, M. S. (1990). Derivation of some modern arc magmas by melting of young subducted lithosphere. *Nature* **347**, 662–665.

Dick, H. J. B. (1989). Abyssal peridotites, very slow spreading ridges and ocean ridge interaction. In: Saunders, A. D. & Norry, M. J. (eds) *Magmatism in the Ocean Basins. Geological Society, London, Special Publications*, **42**, 71–105.

Elburg, M. A. & Foden, J. (1999). Geochemical response to varying tectonic settings: an example from southern Sulawesi (Indonesia). *Geochimica et Cosmochimica Acta* **63**, 1155–1172.

Elburg, M. A., van Bergen, M. J., Hoogewerff, J., Foden, J., Vroon, P. Z., Zulkarnain, I. & Nasution, A. (2002a). Geochemical trends across an arc–continent collision zone: magma sources and slab–wedge transfer processes below the Pantar Strait volcanoes (Indonesia). *Geochimica et Cosmochimica Acta* **66**, 2771–2789.

Elburg, M. A., van Leeuwen, T., Foden, J. & Muhardjo (2002b). Origin of geochemical variability by arc–continent collision in the Biru area, southern Sulawesi (Indonesia). *Journal of Petrology* **43**, 1–24.

Elburg, M. A., van Leeuwen, T., Foden, J. & Muhardjo (2003). Spatial and temporal isotopic domains of contrasting igneous suites in Western and Northern Sulawesi, Indonesia. *Chemical Geology* **199**, 243–276.

Evensen, N. M., Hamilton, P. J. & O'Nions, R. K. (1978). Rare-earth abundances in chondritic meteorites. *Geochimica et Cosmochimica Acta* **42**, 1199–1212.

Foley, S. F., Venturelli, G., Green, D. H. & Toscani, L. (1987). The ultrapotassic rocks: characteristics, classification, and constraints for petrogenetic models. *Earth-Science Reviews* **24**, 81–134.

Frezzotti, M.-L. (2001). Silicate–melt inclusions in magmatic rocks: applications to petrology. *Lithos* **55**, 273–299.

Ghiorso, M. S., Hirschmann, M. M., Reiners, P. W. & Kress, V. C. I. (2002). The pMELTS: a revision of MELTS for improved calculation of phase relations and major element partitioning related to partial melting of the mantle to 3 GPa. *Geochemistry, Geophysics, Geosystems* **3**, 10.1029/2001GC000217.

Gioncada, A., Clocchiatti, R., Sbrana, A., Bottazzi, P., Massare, D. & Ottolini, L. (1998). A study of melt inclusions at Vulcano (Aeolian Islands, Italy): insights on the primitive magmas and on the volcanic feeding system. *Bulletin of Volcanology* **60**, 286–306.

Green, D. H., Schmidt, M. W. & Hibberson, W. O. (2004). Island-arc ankaramites: primitive melts from fluxed refractory lherzolitic mantle. *Journal of Petrology* **45**, 391–403.

Griselin, M. (2001). Geochemical and isotopic study of the Xigaze and Luobusa ophiolite massifs. Ph.D. thesis. Free University Amsterdam, 216.

Gurenko, A. A., Belousov, A. B., Trumbull, R. B. & Sobolev, A. V. (2005). Explosive basaltic volcanism of the Chikurachki Volcano (Kurile Islands, Russia): petrology, geochemistry and volatile loading revealed from inclusions in minerals. *Journal of Volcanology and Geothermal Research* **147**, 203–232.

Harris, D. M. & Anderson, A. T. J. (1984). Volatiles H_2O, CO_2, and Cl in subduction related basalt. *Contributions to Mineralogy and Petrology* **87**, 120–128.

Hauri, E. H. (2002). SIMS analysis of volatiles in volcanic glasses: 2. Isotopes and abundances in Hawaiian melt inclusions. *Chemical Geology* **183**, 115–141.

Hellebrand, E., Snow, J. E., Hoppe, P. & Hofmann, A. W. (2002). Garnet-field melting and late-stage refertilization in 'residual' abyssal peridotites from the Central Indian Ridge. *Journal of Petrology* **43**, 2305–2338.

Hirschmann, M. M. & Stolper, E. M. (1996). A possible role for garnet pyroxenite in the origin of the 'garnet signature' in MORB. *Contributions to Mineralogy and Petrology* **124**, 185–208.

Jochum, K. P., Dingwell, D. B. & Rocholl, A. *et al.* (2000). The preparation and preliminary characterisation of eight geological MPI-DING reference glasses for *in-situ* microanalysis. *Geostandards Newsletter* **24**, 87–133.

Johan, Z. (2006). Platinum-group minerals from placers related to the Nizhni Tagil (Middle Urals, Russia) Uralian–Alaskan-type ultramafic complex: ore-mineralogy and study of silicate inclusions in (Pt, Fe) alloys. *Mineralogy and Petrology* **87**, 1–30.

Kamenetsky, V. & Clocchiatti, R. (1996). Primitive magmatism of Mt Etna: insights from mineralogy and melt inclusions. *Earth and Planetary Science Letters* **142**, 553–572.

Kamenetsky, V. S., Sobolev, A. V., Eggins, S. M., Crawford, A. J. & Arculus, R. J. (2002). Olivine-enriched melt inclusions in chromites from low-Ca boninites, Cape Vogel, Papua New Guinea: evidence

for ultramafic magma, refractory mantle source and enriched components. *Chemical Geology* **183**, 287–303.

Kamenetsky, V. S., Elburg, M. A., Arculus, R. J. & Thomas, R. (2006). Magmatic origin of low-Ca olivine in subduction-related magmas: co-existence of contrasting magmas. *Chemical Geology* **233**, 346–357.

Kent, A. J. R. & Elliott, T. R. (2002). Melt inclusions from Marianas arc lavas: implications for the composition and formation of island arc magmas. *Chemical Geology* **183**, 263–286.

Kogiso, T. & Hirschmann, M. M. (2001). Experimental study of clinopyroxenite partial melting and the origin of ultra-calcic melt inclusions. *Contributions to Mineralogy and Petrology* **142**, 347–360.

Luhr, J. F. (2001). Glass inclusions and melt volcatile contents at Paricutin Volcano, Mexico. *Contributions to Mineralogy and Petrology* **142**, 261–283.

Malitch, K. N. & Thalhammer, O. A. R. (2002). Pt–Fe nuggets derived from clinopyroxenite–dunite massifs, Russia: a structural, compositional and osmium-isotope study. *Canadian Mineralogist* **40**, 395–418.

Manning, C. E. (2004). The chemistry of subduction-zone fluids. *Earth and Planetary Science Letters* **23**, 1–16.

Martin, H., Smithies, R. H., Rapp, R., Moyen, J.-F. & Champoin, D. (2005). An overview of adakite, tonalite–trondhjemite–granodiorite (TTG) and sanukitoid: relationships and some implications for crustal evolution. *Lithos* **79**, 1–24.

Matveev, S. & Ballhaus, C. (2002). Role of water in the origin of podiform chromitite deposits. *Earth and Planetary Science Letters* **203**, 235–243.

McInnes, B. I. A., Gregoire, M., Binns, R., Herzig, P. & Hannington, M. D. (2001). Hydrous metasomatism of oceanic sub-arc mantle, Lihir, Papua New Guinea: petrology and geochemistry of fluid-metasomatised mantle wedge xenoliths. *Earth and Planetary Science Letters* **188**, 169–183.

McKenzie, D. & O'Nions, R. K. (1991). Partial melt distributions from inversion of rare earth element concentrations. *Journal of Petrology* **32**, 1021–1091.

Métrich, N., Allard, P., Spilliaert, N., Andronico, D. & Burton, M. (2004). 2001 flank eruption of the alkali- and volatile-rich primitive basalt responsible for Mount Etna's evolution in the last three decades. *Earth and Planetary Science Letters* **228**, 1–17.

Müntener, O., Kelemen, P. B. & Grove, T. L. (2001). The role of H_2O during crystallization of primitive arc magmas under uppermost mantle conditions and genesis of igneous pyroxenites. *Contributions to Mineralogy and Petrology* **141**, 643–658.

Mysen, B. O. & Boettcher, A. L. (1975). Melting of a hydrous mantle: II. Geochemistry of crystals and liquids formed by anatexis of mantle peridotite at high pressures and high temperatures as a function of controlled activities of water, hydrogen, and carbon dioxide. *Journal of Petrology* **16**, 549–593.

Nakamura, M. (1995). Residence time and crystallization history of nickeliferous olivine phenocrysts from the northern Yatsugatake volcanoes, central Japan; applcation of growth and diffusion model in the system Mg–Fe–Ni. *Journal of Volcanology and Geothermal Research* **66**, 81–100.

Nicholls, I. A. (1974). Liquids in equilibrium with peridotitic mineral assemblages at high water pressures. *Contributions to Mineralogy and Petrology* **45**, 289–316.

Nikogosian, I. K., Elliott, T. & Touret, J. L. R. (2002). Melt evolution beneath thick lithosphere: a magmatic inclusion study of La Palma, Canary Islands. *Chemical Geology* **183**, 169–193.

O'Hara, M. J. (1968). The bearing of phase equilibria studies in synthetic and natural systems on the origin and evolution of basic and ultrabasic rocks. *Earth-Science Reviews* **4**, 69–133.

Pearce, J. A., Barker, P. F., Edwards, S. J., Parkinson, I. J. & Leat, P.T. (2000). Geochemistry and tectonic significance of peridotites from the South Sandwich arc-basin system, South Alantic. *Contributions to Mineralogy and Petrology* **139**, 36–53.

Peccerillo, A., Poli, G. & Serri, G. (1988). Petrogenesis of orenditic and kamafugitic rocks from central Italy. *Canadian Mineralogist* **26**, 45–65.

Petry, C., Chakraborty, S. & Palme, H. (2004). Experimental determination of Ni diffusion coefficients in olivine and their dependence on temperature, composition, oxygen fugacity, and crystallographic orientation. *Geochimica et Cosmochimica Acta* **68**, 4179–4188.

Portnyagin, M. V., Mironov, N. L., Matveev, S. V. & Plechov, P. Y. (2005). Petrology of avachites, high-magnesian basalts of Avachinsky Volcano, Kamchatka: II. Melt inclusions in olivine. *Petrology* **13**, 358–388.

Ramsay, W. R. H., Crawford, A. J. & Foden, J. D. (1984). Field setting, mineralogy, chemistry, and genesis of arc picrites, New Georgia, Solomon Islands. *Contributions to Mineralogy and Petrology* **88**, 386–402.

Reubi, O., Nicholls, I. A. & Kamenetsky, V. S. (2002). Early mixing and mingling in the evolution of basaltic magmas: evidence from phenocryst assemblages, Slamet Volcano, Java, Indonesia. *Journal of Volcanology and Geothermal Research* **119**, 255–274.

Roedder, E. (1984). *Fluid Inclusions. Mineralogical Society of America, Reviews in Mineralogy*, **12**, pp. 646.

Rohrbach, A., Schuth, S., Ballhaus, C., Münker, C., Matveev, S. & Qopoto, C. (2005). Petrological constraints on the origin of arc picrites, New Georgia Group, Solomon Islands. *Contributions to Mineralogy and Petrology* **149**, 685–698.

Schiano, P., Eiler, J.M., Hutcheon, I. D. & Stolper, E. M. (2000). Primitive CaO-rich, silica-undersaturated melts in island arcs: evidence for the involvement of clinopyroxene-rich lithologies in the petrogenesis of arc magmas. *Geochemistry, Geophysics, Geosystems* **1**, 1999GC000032.

Schuiling, R. D. (2004). Thermal effects of massive CO_2 emissions associated with subduction volcanism. *Comptes Rendus, Geoscience* **336**, 1053–1059.

Sisson, T. W. & Bronto, S. (1998). Evidence for pressure-release melting beneath magmatic arcs from basalt at Galunggung, Indonesia. *Nature* **391**, 883–886.

Sisson, T. W. & Layne, G. D. (1993). H_2O in basalt and basaltic andesite glass inclusions from four subduction-related volcanics. *Earth and Planetary Science Letters* **117**, 619–635.

Smith, D. R. & Leeman, W. P. (2005). Chromian spinel–olivine phase chemistry and the origin of primitive basalts of the southern Washington Cascades. *Journal of Volcanology and Geothermal Research* **140**, 49–66.

Sobolev, A. V., Dmitriev, L. V., Barsukov, V. L., Nevsorov, V. N. & Slutsky, A. B. (1980). The formation conditions of high magnesium olivines from the monomineralic fraction of Luna-24 regolith. *Geochimica et Cosmochimica Acta* 105–116.

Sobolev, A. V., Hofmann, A. W. & Nikogosian, I. K. (2000). Recycled oceanic crust observed in 'ghost plagioclase' within the source of Mauna Loa lavas. *Nature* **404**, 986–990.

Stix, J., Layne, G. D. & Williams, S. N. (2003). Mechanisms of degassing at Nevado del Ruiz volcano, Colombia. *Journal of the Geological Society, London* **160**, 507–521.

Straub, S. M. & Layne, G. D. (2003). Decoupling of fluids and fluid-mobile elements during shallow subduction: evidence from halogen-rich andesite melt inclusions from the Izu volcanic arc front. *Geochemistry, Geophysics, Geosystems* **4**, 2002GC000349.

Sun, S.-s. & McDonough, W. F. (1989). Chemical and isotopic systematics of oceanic basalts: implications for mantle composition

and processes. In: Saunders, A. D. & Norry, M. J. (eds) *Magmatism in the Ocean Basins. Geological Society, London, Special Publications* **42**, 313–345.

Tamura, Y. & Tatsumi, Y. (2002). Remelting of an andesitic crust as possible origin for rhyolitic magma in oceanic arcs: an example from the Izu–Bonin arc. *Journal of Petrology* **43**, 1029–1047.

Tamura, Y., Yuhara, M. & Ishii, T. (2000). Primary arc basalts from Daisen Volcano, Japan: equilibrium crystal fractionation versus disequilibrium fractionation during supercooling. *Journal of Petrology* **41**, 431–448.

Tepley, F. J., Davidson, J. P., Tilling, R. I. & Arth, J. G. (2000). Magma mixing, recharge and eruption histories recorded in plagioclase phenocrysts from El Chichón Volcano, Mexico. *Journal of Petrology* **41**, 1397–1411.

Turner, S., George, R., Jerram, D. A., Carpenter, N. & Hawkesworth, C. J. (2003). Case studies of plagioclase growth and residence times in island arc lavas and a model to reconcile discordant age information. *Earth and Planetary Science Letters* **214**, 279–294.

Zanetti, A., Tiepolo, M., Oberti, R. & Vannucci, R. (2004). Trace-element partitioning in olivine: modelling of a complete data set from a synthetic hydrous basanite melt. *Lithos* **75**, 39–54.

APPENDIX: MODELLING OF CAO LOSS TO OLIVINE

The distance–CaO concentration gradient in the olivine around the inclusion was described by the function $C = C_{\text{int}} + (C_0 - C_{\text{int}})\text{erf}(x/2\sqrt{Dt})$, which is the solution to diffusion in a semi-infinite medium with constant surface concentration (Albarède, 1995). C_0 was taken to be the CaO content at an 'infinite' distance from the melt inclusion, and C_{int} was taken as the CaO content closest to the inclusion. The value for Dt was adjusted to match the calculated profile to the observed one. The actual values for D and t are of no consequence for this model. The amount of CaO lost to the olivine can be calculated from a hypothetical 'boundary layer', which is a layer with a thickness $\partial = 2\sqrt{Dt/\pi}$ with a homogeneous concentration C_{int}. This is the analytical equivalent of calculating the surface under the diffusional profile from $x = 0$ and $x = \infty$, and C_{int} to C_0. Therefore, the amount of CaO lost to the olivine is $\text{CaO}_{\text{lost}} = (4/3)\pi(\partial - r)^3(C_{\text{int}} - C_0)$, with r being the radius of the melt inclusion. The original CaO concentration of the melt inclusion is then $[(4/3)\pi(r)^3\text{CaO}_{\text{melt}} + (3{\cdot}25/2{\cdot}77)\ \text{CaO}_{\text{lost}}]/(4/3)\pi(\text{r})^3$. The factor $(3{\cdot}25/2{\cdot}77)$ accounts for the assumed density difference between the melt inclusion and the olivine.